

## ***RESULTS***

Mango inflorescence is a raceme developing from axillary and terminal buds of the branches in the floral season (December to February). It is a large panicle containing numerous tiny flowers with reddish white or yellowish green colour. Staminate and hermaphrodite flowers are borne on the same panicle. Along with the normal growing vegetative shoots and panicles, trees also exhibit shoots and inflorescences which are morphologically and developmentally different from the normal ones. These two stages of growth characterize the disease, vegetative malformation and floral malformation disease. The typical symptoms of floral malformation represent stunted and thick panicle axis, abnormal size of flowers, occurrence of large number of unopened flowers, shift to more staminate flowers and abortive essential organs. Rarely panicles may bear fruits which do not develop further after reaching pea stage.

### **3.0 Occurrence of Floral malformation in and around Baroda :**

The survey of various mango orchards in and around Baroda revealed the prevalence of floral malformation in many trees. The percentage occurrence of the disease ranged from 10 to 50% in different orchards (Fig. 1). During the survey, floral malformation was encountered in eight varieties of mango trees falling under the age group of 8 to 30 years viz. Rajapuri, Kesar, Ladva, Limdi, Langra, Alphonso, Dadamio and a local variety growing in different orchards.

#### **3.1.0 Morphological Observations :**

##### **3.1.1 Floral Malformation :**

Malformed panicles (Fig. 2B) can be easily differentiated from healthy ones (Fig. 2A). The number of flowers in each lateral branch of malformed panicle axis increases and the internodes shorten giving a bunched appearance to the panicles. The number of sepals and petals in staminate as well as bisexual flowers increases from five to seven in malformed inflorescences varying with the variety. The size of petals and sepals also increases in diseased flowers. Usually there is a single fertile stamen in healthy flowers but its number may increase to two in abnormal flowers of Rajapuri, Ladva and Langra varieties. In bisexual malformed flowers glandular disc segments also increase numerically from five to seven in Ladva and five to six in Limdi and Langra. However,

the gland has only four segments in malformed staminate flowers of variety Limdi and Langra compared to five segments of gland in the respective healthy varieties.

The number of staminate flowers increases when an inflorescence is malformed. All the varieties studied possess less percentage of bisexual flowers among malformed panicles except in Kesar (Fig. 3). The flowers are usually penta to hexamerous, while in healthy panicles they are tetra to pentamerous. Male and bisexual flowers of affected panicles (Fig. 4B) irrespective of the variety are larger in size than the healthy ones (Fig. 4A). The average length and width of flowers vary from 3.5 to 5 mm and 5.5 - 7 mm in malformed panicles while it is 3.5 to 4.5 mm and 5-6 mm in healthy panicles of Rajapuri respectively (Table 4). The aestivation of calyx and corolla also varies between flowers of healthy and malformed inflorescences. The whorls of the former are arranged in imbricate manner while in the latter the arrangement is quincuncial. The essential and non-essential organs of flowers of malformed panicles vary dimensionally compared to healthy ones in *M. indica* var Rajapuri. The main axis of the inflorescence (peduncle) and the stalk bearings the flowers (pedicel) are relatively thick in malformed ones. Similarly the size of the sepals, petals, staminodes, anthers, pollengrains, ovary, glandular disc is relatively larger in flowers from malformed inflorescences (Table 1).

Onset of young panicles starts from terminal and axillary buds during mid-December. Morphologically two types of terminal buds are distinguished; one elongated stout with large sized leafy bud scales and the other with only a few open small bud scales (Fig. 5A). The former contains black resin deposits on the bud scales and eventually may develop into malformed panicles (Fig. 5B). During January most of the remnant vegetative malformed twigs of the previous year produce young malformed panicles as well as young vegetative malformed shoots (Fig 5C). In some instances they produce only malformed panicles. Although the emergence of malformed panicles and healthy panicles occurs at the same time. Among the malformed panicles the blooming of male flowers is much earlier compared to the bisexual ones.

Malformed panicles have a short axis measuring about 21 cms in length while in healthy the length ranges from 27 to 50 cms. The axis or peduncle is considerably thick with a diameter ranging from 0.8 to 1.0 cm. In healthy ones the diameter does not reach

beyond 0.6 cm

Malformed panicles generally develop in groups from axillary buds forming multiple panicles. The axillary bud meristems at the terminal position of the shoot become activated and produce several panicles forming a bunch.

The axis of the malformed panicles is often noticed with injuries caused by the insect borers. Few insects are also found feeding on the young leafy and fleshy bracts of the flowers. The morphology of these insects reveal that they are thrips. It is apparent that both abaxial and adaxial sides of bract are extensively damaged by these thrips. Although these thrips are not found carrying any spores of *Fusarium moniliforme* or any other fungal propagules, they cause considerable damage to the floral bracts.

Interestingly, macro and micro conidial structures and hyphal mat are often found associated with the lesions on the sepals and rarely on the petals. Some of the malformed panicles developed at the later part of floral season i.e. during February-March bear large bracts resembling a leaf (Fig. 6A,B). Unlike healthy panicles, malformed panicles bear fruits which do not develop more than a pea size and shed-off early.

### 3.1.2 Vegetative Malformation :

Vegetative malformation is characterised by the development of many stunted axillary shoots from axillary buds as well as the terminal bud of the shoots (Fig. 7A). The dwarf vegetative shoots (Fig. 7B) often form a bunch. The axillary shoots in the cultivar Rajapuri are 2-6 cms in length and 0.2 to 1 cm in thickness. Such shoots further bear tiny shoot-lets with length and thickness varying from 1.5-3 cms and 0.2 to 0.4 cms respectively.

Many bunches appearing on the branches represent a typical symptoms of vegetative malformation known as 'bunchy top'. The leaves from bunchy top shoots are reduced in length (measuring from 8.5 to 12.5 cms) while shoot-lets bear leaf scales with length ranging from 2.5 to 3 cms. Leaf bases and bud scales show lesions with dark

blackish gum resin secretions. These shoots are often injured by insect borers resulting in pith rot and subsequently dry as in diseased panicles. However, axillary buds of bunched top shoots being active for most part of the year recurrently produce vegetative shoots.

During the floral season vegetative malformed shoots give rise to malformed panicles. The axillary and terminal buds of affected shoots have minute openings at their tips surrounded by lesions (Fig. 8 A,B). Such buds are often found associated with microscopic phytophagous insects, the mites. The young and adult mites (Fig. 8C,D) are located in closed as well as open buds of the bunched top shoots. The adult mites are frequently located in the axillary buds and the senescing affected shoots. Such adult mites are noticed with micro, macroconidia and hyphae (Fig. 8E) of *Fusarium moniliforme* on their entire body surface. Most of the buds and bud scales are noticed feeding by the mites and some insect borers are found in rotting or necrotic portions of the buds and shoots. The following categories of mites isolated from the buds and shoots are identified.

- 1) Phytoseiid mite predators: These mites are commonly found feeding on or associated with phytophagous and other insects.
- 2) Cryptostigmatids : These mainly help in degradation/decomposition of organic matter and are very few plant feeders. A few other members of mites isolated from vegetative malformed buds are identified as 1) *Aceria mangifera* Sayed, 2) *Cheletogenes* sp 3) *Cunaxoides* sp., 4) *Tydeus* sp., and 5) Tenuipalpid mite,

### **3.2.0 Histological and Histochemical Studies :**

#### **3.2.1 Terminal buds :**

Terminal buds of shoots in an annual cycle have been studied to determine the following: i) the pathogen interaction at different developmental stages of the host ii) a possible role of the pathogen in two different phases of disease development i.e. vegetative and floral malformation symptoms of the disease as the apical meristems from the precursors of floral or vegetative buds.

Shoot apices of *Mangifera indica* var. Rajapuri have single layered tunica covering an undifferentiated corpus zone. The epidermal cells of leaf primordia for a major part of the year are noticed with phenolic contents. During winter shoots usually bear reproductive and vegetative apices. However, the development of reproductive apices is predominant in this season which commences in the last week of December and concludes in February.

Reproductive apices have characteristic elongated axis bearing axillary floral bud meristems (Fig. 9A). The cells of the apical and axillary bud meristems possess dense cytoplasm and large nucleus. Besides tunica and corpus further zonation is not distinguishable. Procambial layer, however, is distinct and often gets separated in the region below the corpus zone due to development of gum-resin ducts.

A few fragments of pathogenic hyphae near the meristem are noticed in December. In January hyphal filaments are often found in the vicinity of the apex and noticed passing through the adjacent overlapping young bract primordia close to the apex (Fig. 9B,C). Some intercellular mycelium is also noticed at the base of the axillary floral meristem. Floral meristems are found invaded by hyphae on the tunica layer and attached to the bract primordia (Fig. 9D,E).

During summer and monsoon the shoots invariably bear vegetative apices. These apices are characterized by a wide dome shaped structure with dormant axillary meristems. The main axis of the apex is highly reduced with distinct tunica-corporis zonation.

In early summer (March and April), spores of *Alternaria* sp., and *Torula* sp. along with mycelium of the pathogen often attached to leaf primordia appear to induce phenolic contents in the host (Fig. 9F). The intercellular mycelium is also noticed in the leaf primordia. Tuft of mycelium or hyphal aggregates are commonly found attached to the leaf primordia, rarely even encircle the propagules of *Alternaria* sp. and *Torula* sp. Pathogen appears to enter the shoot mainly through the base of the leaf primordia attached with the meristem (Fig. 9G). The proliferation of hyphae further into shoot appears to be intercellular (Fig. 9H).

When stained with chlorazol black 'E' the epithelial cells of gum-resin ducts of shoot and leaf primordia appear jet black while the gum-resin secretion exhibits dark to pale brown colour. Phenolic contents also stained similar to resin secretions. Although resin and phenolic contents are not noticed in the young bracts of floral season but during rest of the winter and early summer i.e. in December, March and April respectively, the accumulation of phenolic contents are high. It appears that infection in apices is higher in March which is reflected by the copious accumulation of resin secretion in the duct lumen (Fig. 10A) of shoot. Phenolic deposits are also found accumulating in the pith cells of shoot and mesophyll cells of young leaves.

During mid-summer i.e. May the vegetative apices show typical characters of dormancy. The tunica layer is darkly stained and corpus zone contain group of less densely stained cells, some of which are highly vacuolated (Fig. 10B). The number and relative length of leaf primordia are reduced. These apices do not show any traces of pathogen either in mat form or hyphae or propagules near the apex or in between the young leaf primordia.

The vegetative apices in June are active and covered with relatively more number of leaf primordia. The tunica and corpus zone are densely stained. Propagules of *Alternaria* sp. and hyphae of *Fusarium moniliforme* are also noticed attached to the leaf primordia lying close to the meristem. Resinous secretions are not found in the shoots during May and June (Fig. 10C). However, in June phenolic contents are noticed in mesophyll of leaf primordia.

During Monsoon (July, August and September) insect remains (Fig. 10D,E) are predominantly seen near the vegetative apex. The tunica layer of apical meristem appears wavy and bud meristems are not active while the vegetative apices appear to be dormant in August and September. Such apices appear condensed dome like having phenolic contents in some of the parenchyma cells below corpus zone. The entry of the pathogen into shoot cells below the meristem is similar as in April. The insect remains near the apical meristem are relatively more in September.

Phenolic contents and resinous secretions gradually increased in shoots from July to September. The cells of epidermis, cortex and pith have relatively more phenolic deposits. The gum-resin duct lumen in the pith cells of shoot are filled with secretory material.

The shoots mainly bear typical vegetative apices during October and November. Such apices are flat dome shaped and are associated with hyphae near the meristem. There is no accumulation of phenolic contents in the cells below the corpus zone as in earlier months. However, in November the tunica layer of apical meristem is severely infested and degraded by pathogen (Fig. 10F). This infected zone including subtended leaf primordial tissue is marked by phenolic accumulation. However, propagules of *Alternaria*, *Torula* and a few insect remains are noticed near the apex and leaf primordia. Bud meristems are also infected and the site of infection is at the base of leaf primordia. Apices in both these months have phenolics confined to mesophyll cells of leaf primordia but abundantly distributed in epidermis, cortex and pith cells of shoot. Duct's lumen in pith has less secretion of gum-resin.

The terminal buds in general have many clustered ducts in the shoot which are 2-3 mm away from the apical meristem. During January to February the shoots mainly bear floral apices. The duct lumen diameter in these shoots is maximum. However, in February the percentage area and frequency (FR) of ducts is reduced. During this period air temperatures declines reaching a minimum of 12.8°C (January) and humidity of 67% and 61% in January and February respectively. The maximum temperature recorded ranges from 27.6°C - 31.2°C and minimal from 12.8°C to 20.7°C.

During summer the infection declines and parallelly the duct lumen diameter (LD) becomes reduced. The season recorded relatively high temperature of 39.7°C with lowest humidity (49%) of the year in April (Fig. 11). Increment in mean lumen diameter of the ducts resumes again in August as well as in November months. It is apparent that the high incidence of infection goes hand in hand with increased lumen diameter of these ducts (Table 2).

### 3.2.2.0 Terminal buds : Histochemistry

3.2.2.1 Starch: The deposition of total insoluble polysaccharides (mainly starch) is confined to the pith cells of shoot. Starch accumulation is relatively high during early floral season i.e. in the last week of December (Fig. 10G) and starch grains are often masked by phenolic contents. The deposition of these contents is less in January but appear more in February (Fig. 10H). During summer and monsoon these deposits are totally absent in the pith parenchyma. The starch reserves gradually increase from September onwards until December.

3.2.2.2 Total proteins: The nucleus is stained irrespective of the tissues of the shoot apex. The cells of the meristem invariably of the season are densely stained. With the inception of winter in December, protein deposits in leaf primordial tissues and shoot apical meristem start depleting. During floral season only few epidermal cells of leaf primordia accumulate these reserves.

The accumulation of protein bodies are found to be more in the vegetative apices of late winter and early summer i.e. March and April. The increased accumulation of these deposits runs parallel with increase in intensity of infection in both these months. The leaf primordial epidermis and mesophyll cells show few protein bodies. Parenchyma around the resin ducts also show few such reserves in both the months. The pith ducts of shoot also reveal proteinaceous resin content (Fig. 12A). Some of the cells in the shoot are noticed with both phenolics as well as protein contents during these months.

During summer the shoots show only few cells with prominently stained nucleus. Further excluding leaf primordial epidermis and mesophyll, protein deposits do not accumulate in shoot parenchyma or the resin ducts.

The nucleus in the shoot cells resumes dense stainability during July to September (Monsoon) unlike in summer. The leaf primordial tissue shows gradual increase in protein deposits in the mesophyll cells and accumulates heavily in September with the increasing incidence of infection. A few layers below corpus zone, some parenchyma in the shoot have phenolic deposits as well as protein filled cells (Fig.

12B). However, there are no protein deposits or densely stained cells either in leaf primordia or shoot pith resin ducts from July to September.

In October and November, besides few parenchyma below corpus zone there are no protein bodies either in the duct lumen of leaf primordia or shoot.

**3.2.2.3 Total lipids :** In all the seasons the apical meristem (Fig. 12C) along with the subtending leaf primordia have relatively more lipid bodies except in the meristems of October and November. A few pith cells of shoot accumulate phenolic contents and lipid bodies in November (Fig. 12D).

#### **3.2.3.0 Floral Malformation :**

Sections taken from peduncle, pedicel, essential and non-essential organs of flowers at different stages of growth in malformed and healthy inflorescences have been studied under microscope for histological details.

**3.2.3.1 Peduncle:** The epidermis is wavy forming prominent ridges and furrows. The cells are covered by a thick layer of cuticle which often extends over the lateral walls (Fig. 12E). Cortical and pith cells are larger with diameter ranging from 35 to 53  $\mu\text{m}$  in the former and from 37 to 72  $\mu\text{m}$  in the latter. Although intra and intercellular hyphae (Fig. 12F) appear rarely in the cortical region, phenolic contents are often noticed in the host cells. A cap-like thick walled perivascular fibres (Fig. 12G) are found surrounding each primary gum-resin duct. These fibres are not much elongated but are usually thick walled. Their length vary from 589 to 1358  $\mu\text{m}$ . Gum-resin ducts are arranged away outside the vascular tissue. The ducts among this ring have reduced lumen diameter (Table 3) with no resin secretion (Fig. 12H). Xylem also forms a continuous ring showing secondary growth in the peduncle. The outermost vessels are radially flattened or sometimes irregularly shaped. Occasionally tyloses are noticed in the vessel elements. The frequency of vessels is relatively higher in the xylem (Table 3). The intervessel bordered pits are scalariform and alternate type. Ray and axial parenchyma cells of phloem show relatively few cells accumulated with phenolic contents.

### 3.2.3.2 Young and Mature Pedicel :

Mycelia of *Fusarium moniliforme*, *Curvularia* and *Alternaria* sp. are often found associated with the epidermis of malformed pedicels. Hyphae of *F. moniliforme* are frequently found associated with the bracts. The cortical and pith cells are enlarged. In mature pedicel the epidermis is covered by a thick cuticle of 1.6–4.8  $\mu\text{m}$  thickness. The gum-resin ducts appear relatively larger with lumen diameter ranging from 32 to 181  $\mu\text{m}$ . The parenchyma cells lying between the primary and secondary gum-resin ducts often undergo disintegration leading to the confluence of lumen of both the ducts (Fig. 13A). The vessel element frequency is higher (Table 3) ranging from 24–54 per sq.mm. Occurrence of intercellular hyphae and accumulation of phenolic contents are rarely in cortex and pith. The sections of samples from malformed panicles reveal the close association of fungus with the organs of young and mature floral buds and with the essential organs of open flowers.

### 3.2.3.3 Young Buds :

Longitudinal sections of young buds measuring 0.7 mm in diameter (Table 4) from malformed inflorescence have revealed the association of fungus with all floral organs. Mycelial fragments are often found in the narrow space between the overlapping sepals and petals. Mycelia often appear in groups forming a mat-like structure. In resin embedded semithin sections mycelial mat appears as a pile or row of hyphae or microconidia of *Fusarium moniliforme* (Fig. 13B). The entry of the pathogen into these buds appears to be followed by necrosis of sepals and petals (Fig. 13C). Hyphal filaments of the pathogen have also been noticed in close association with the ovary and anther wall (Fig. 13D). Mycelia often appear in the anther locule at microspore mother cell phase. The hyphae are also noticed attached to the ovular chamber at this stage.

Young buds of healthy panicles measure comparatively less in size (Table 4) than those of malformed ones and are free of pathogen association.

### 3.2 3.4 Mature Buds :

The buds of Rajapuri cultivar collected from fully developed malformed panicles measure nearly twice in size compared to those in healthy panicles (Table 4). The mycelial filaments are prominent and often appear inbetween sepals and petals. Hyphae are also noticed in close association with the surface of the ovary and gland.

Anthers are tetralocular and dorsifixed with a filament that undergoes necrosis at the point of attachment with the anther. The cuticle covering the epidermal layer of anther is thicker and ribbed.

A thick mat of *Fusarium* hyphae is consistently noticed in the basal groove of anther lobe where the filament is connected (Fig. 13E,F). In a few instances fusarial mat appears close to the disorganised filament (Fig. 13G,H). The fungus seems to enter into the anther locule (Fig. 14A,B) from the base of the anther lobes where the filament is attached or directly anther lobes pass through the anther epidermis (Fig. 14C). The cells at the base of anther lobes appear thick walled and filled with phenolic contents. The pollen grains are usually round and exhibit thin cell walls. However, in the variety Langra, pollen grains appear oval-elliptical in shape. The severely infected anthers of all varieties studied show loss of cell identity in the tapetal layer followed by phenolic accumulation (Fig. 14D). Such infected anther locule is found filled with darkly stained pollen grains and fragments of mycelia (Fig. 14E,F). Pollen grains with attached fungal hyphae are frequently found in the locule (Fig. 14G,H). In some cases pollen grains appear with thin wavy walls and empty due to plasmolysed cytoplasm (Fig. 15A) in comparison to healthy pollen with dense cytoplasm (Fig. 15B).

In the healthy panicles anthers are free from fusarial association and lesions with phenolic accumulations in the cells (Fig. 15C). The tapetal cells around the anther locule appear distinct and the pollen grains are usually round in all the varieties.

The sessile ovary is attached with a lateral style and an anatropous ovule is arranged on a basal placenta. The style is slender and short with a bifid stigma. Stigma consists of a narrow opening of 4-5 cells deep (Fig. 15D,E). The longitudinal sections

passing through style of uninfected flowers reveal that it is composed of compactly arranged transmitting tissue which is continuous with the ovary wall. While in infected flowers, it shows lesions characterized by the darkly stained cells. These lesions extend from stigmatic groove to the ovular chamber through the length of the style. (Fig. 16A). Fusarial mat is also noticed at the opening of the stigmatic groove (Fig. 16B). In the severely infected flowers this leads to the formation of a canal in the style opening into the ovular chamber. The fungus in the form of filaments and mat often occur along the canal (Fig. 16C). The ovary wall besides style also consists of lesions characterised by the phenolic containing cells. These lesions also appear across the ovary wall from outer to the inner surface (Fig. 16D). Thus the invasion of *Fusarium moniliforme* into the ovule appears to be mainly occurring through the stylar transmitting tissue or directly through the ovary wall.

Hyphal fragments and mat are also found in the ovular chamber often attached to the surface of the ovule and inner layer of ovary wall (Fig. 17E,F) These infection sites too accumulate phenolic contents either in the intercellular spaces or entire cell lumen and form lesions which are associated with hyphal filaments. The ovule seems to be invaded by the pathogen either at the micropylar end (Fig. 17A,B&C) or directly through the wall layers. The mycelium of *Fusarium* is noticed proliferating intercellularly in the ovary wall surrounding it (Fig. 17D).

### 3.2 3.5 Open Flowers

Malformed flowers usually appear larger than the healthy ones (Table 4). The blooming of buds of malformed panicles is much delayed and relatively few buds open as compared to healthy ones. The open flowers also show similar mode of distribution of fungus in the essential organs as described in mature buds. However, open flowers from malformed as well as healthy panicles generally show dehisced anther locules lodged with a few pollen grains. The anther locules in flowers of malformed inflorescence are filled with necrotic cells extensively deposited with phenolic contents and fusarial mat.

Severely infected flowers are noticed containing irregularly shaped ovule completely filled with dark contents (Figs.15D,17G,H) Heavy deposition of phenolic

contents along with fusarial mat (Figs 15F;17G) conidiophores (Fig.17H) and microconidia are also found associated with the ovary wall, stylar tissue cells and ovule.

The glandular segments form the base of the receptacle in bisexual and male flowers of both malformed and healthy panicles. The surface of the gland shows ridges and furrows in both the panicles. The secretory epithelium of malformed gland consists of columnar cells which are densely stained indicating abundant secretion. The columnar cells often lose their identity and accumulate phenolic compounds (Fig. 17I). Gum-resin ducts are in a ring anastomosing into the parenchymatous pedicel. The duct lumen is often filled with gum-resin secretion.

#### **3.2.4.0 Floral Malformation : Histochemistry**

The epidermal (Fig. 18A) and cortical cells (Fig. 18B) close to the infection sites of the peduncle accumulate phenolic derivatives of catechin type. Gum-resin secretion do not show such type of phenolic contents

**3.2.4.1 Starch:** The deposition of these polysaccharides are not noticed in any tissues of the peduncle. Pedicels, sepals and petals of buds show less accumulation of starch. The filament of anthers at the infection sites (Fig. 18C) is noticed with more starch granules compared to other portion of the filament. The pollen grains are filled with starch deposits (Fig. 18D) while ovary tissues are devoid of such reserve material

**3.2.4.2 Total proteins:** The total proteins appear as tiny to large granular blue coloured bodies. Epidermal cells, pith parenchyma and gum-resin canal epithelial cells of the peduncle show relatively more proteins (Fig. 18E) In pedicel protein bodies accumulate only in the epidermis. The cells near the basal groove of the anther lobes which also represent an infection site, show more accumulation of these reserves (Fig.18F). Although columnar cells of the glandular disc show more deposition of protein bodies, ovary wall and ovule are free of reserve metabolites.

**3.2.4.3 Total lipids** The cuticle of peduncle stains densely with sudan black 'B' compared to that of healthy. However, cortical cells have scanty lipid globules.

Paratracheal parenchyma, ray cells and phloem parenchyma accumulate these reserve materials (Fig. 18G,H). The pedicel shows scanty deposition of sudan black on the cuticle and cortical cells but gum-duct lumen is filled with lipid secretion (Fig.19A). In young and mature buds lipid globules are found only in pollen grains. The cells of the ovary do not show any accumulation of lipid bodies.

3.2.4.4 Succinic Dehydrogenase Enzyme : Epidermis, cortex (Fig.19B) and perivascular fibres (Fig. 19C) show intense reaction product of the dehydrogenase. The enzyme precipitation is noticed in the paratracheal parenchyma (Fig. 19D), phloem and pith parenchyma cells. The gum-resin duct lumen and the epithelial cells around it are devoid of enzyme reaction product. The cortical cells of pedicel (Fig. 19E) exhibit relatively more enzyme activity than the peduncle. The vascular tissues of pedicel also reveal this enzyme activity. In the anther epidermal cells show faintly stained dehydrogenase enzyme reaction product (Fig. 19F). The stilar transmitting tissue, ovary wall and ovule do not show dehydrogenase activity

3.2.4.5 Peroxidase Enzyme Peroxidase activity is noticed in the peduncle particularly at the infection sites (Fig. 19G) i.e. epidermal cells and hypodermal cells. Perivascular fibres covering the vascular tissue lying in the inner cortex show a faint reaction of the enzyme. Few parenchyma surrounding the vessel elements exhibit granular accumulation representing a positive site of enzyme distribution (Fig. 19H). Some of the pith parenchyma are also noticed with enzyme precipitation lining the inner sides of cell walls facing the cytoplasm (Fig. 20A). In the pedicel except for few inner cortical cells, (Fig. 20B) the epidermal cells, the vascular tissue and pith parenchyma do not exhibit the reaction product of the enzyme. Further, the infection sites of the anther (Fig. 20C) i.e., the basal groove where the filament is attached and the anther wall (Fig. 20D) in between two anther lobes exhibit intense peroxidase reaction. In ovary, the stilar transmitting tissue (Fig. 20E) as well as ovular cells (Fig. 20F) show dense oxidase enzyme precipitation.

#### 3.2.5.0 Healthy Panicles :

The healthy panicles are characterised by slender elongated peduncle bearing normal flowers

3.2.5.1 Peduncle : Epidermal cells are covered with relatively thin and uniform cuticular layer. The cuticle does not extend into lateral epidermal cell walls (Fig. 20G). Cortical and pith cells are round to oval measuring 26 to 37  $\mu\text{m}$  and 26 to 43  $\mu\text{m}$  respectively. The cortical fibres are relatively longer measuring 745 to 2077  $\mu\text{m}$  in length. Secondary growth is not apparent in the peduncle. Elements of proto and metaxylem constitute the xylem. The gum-resin ducts have larger lumen diameter (Table 3) and contain relatively more dark contents (Fig. 20H). Parenchyma cells of phloem show more phenolic contents. The frequency of tracheary elements is relatively less (Table 3). The length of metaxylem vessel elements ranges from 56 to 186  $\mu\text{m}$  and the width from 31 to 59  $\mu\text{m}$ .

3.2.5.2 Pedicel: The association of pathogen with the pedicel is not found . In mature pedicel, the epidermis is covered by relatively thin cuticle ranging from 1.6 - 4.8  $\mu\text{m}$  in thickness (Table 3). The phloem gum-resin ducts are arranged away from the vascular tissues. The duct lumen diameter ranges from 32-88  $\mu\text{m}$  (Table 3). The frequency of tracheary elements is less (Table 3) ranging from 12 to 30 per sq. mm.

3.2.5.3 Bud: Young buds are devoid of phenolic deposition in sepals, petals and receptacle vascular traces. The density of trichomes is less in the pedicels of mature buds. Secretory material is not found in the lumen of the ducts of receptacle zone. Glandular epithelium (columnar cells) is devoid of phenolic deposition.

3.2.5.4 Flower: The non-essential organs like sepals, petals, staminodes are free from the pathogen. At young stages, anther epidermis is continuous and endothelial fibrous layer is prominent with wall thickenings. The tapetal cells are also prominent in the anther locule (Fig. 21A). The tissues of ovary do not show association of hyphae, lesions or accumulation of phenolic contents. The secretory cells of gum ducts are dense but no secretory material is found in the duct lumen.

### 3.2.6.0 Healthy Panicles : Histochemistry

The epidermal cells and the outermost cortical cells of peduncle exhibit hydrolysable tannins, however, catechin type of phenolic derivatives are absent in these cells. The secretory material in the ducts do not show any of these phenolic contents.

However, the secretory cells do show tannins.

3.2.6.1 Starch: Starch grains are relatively more in the cells of epidermis, cortex (Fig. 21B) and pith duct cells of peduncle. Starch is commonly found in the young buds, pedicel, sepals and organs of young and mature buds

3.2.6.2 Total proteins: The cells of epidermis, cortex and gum-resin ducts of peduncle show no protein bodies (Fig. 21C). Protein bodies are found in the epidermal cells of pedicel. The base of anther lobe near the filament shows no protein deposits. The gland cells of the flowers show few protein bodies in the secretory cells.

3.2.6.3 Total lipids Cortical cells have more deposition of lipids while paratracheal parenchyma (Fig. 21D) do not accumulate these reserve material. A few lipid bodies are found in phloem parenchyma. Lipid globules are found in the pollen grains of young and mature anthers. Ovary wall and ovule do not accumulate lipids.

3.2.6.4 Succinic Dehydrogenase: The epidermis, cortex and perivascular fibres of peduncle exhibit relatively less enzyme localisation. Further vascular tissue of peduncle (Fig. 21E), also show scanty reaction product of the enzyme. In healthy pedicel, the enzyme is localised in a few cortical parenchyma but the vascular tissue and pith parenchyma are noticed with relatively less enzyme precipitation. Intense reaction product of dehydrogenase enzyme is found in the epidermal cells of basal groove of anther lobe. The reaction product of dehydrogenase (Fig. 21F) appears as large globules in the cytoplasm of the cells. But the ovary, stylar transmitting tissue, ovary wall cells and ovule do not show any enzyme activity

3.2.6.5 Peroxidase: The heat treated peduncle does not exhibit the enzyme reaction product (Fig. 21G) The lumen of cortical cells and its cell walls in peduncle show intense reaction of this oxidase (Fig. 21H). Perivascular fibres show similar reaction of the enzyme as noticed in malformed peduncle. Paratracheal parenchyma (Fig. 22A) do not show any enzyme precipitation. The enzyme activity, however, is found along the cell corners of pith parenchyma (Fig. 22B). The enzyme activity in pedicel is similar to that found in malformed ones

### **3.2.7.0 Vegetative malformation :**

3.2.7.1 Malformed shoot : A thick cuticle of 20-24  $\mu\text{m}$  in thickness covers the epidermis and often extends on the radial walls. Cortical parenchyma are larger and radially elongated with a diameter ranging from 32-96  $\mu\text{m}$ . Most of the parenchyma cells in cortex are filled with phenolic contents. The outer cortex is composed of continuous band of 2-3 layers of lignified sclerids (Fig. 22C). There are two distinct rings of gum-resin ducts with the outer ring representing primary ducts which are surrounded by relatively less lignified perivascular fibres in the cortical region (Fig. 22D). The inner ring of resin ducts are found in the phloem produced during secondary growth. The two rings of ducts are separated by the darkly stained primary phloem elements which have undergone obliteration due to secondary growth. The primary duct lumen is often noticed with gum-resin accumulation. Their lumen diameter is slightly less than that of healthy shoots (Table 5). Vessel elements are mostly solitary and rarely appear in radial multiples. The vessel lumen diameter is relatively less in malformed shoots but their frequency is found to be more (Table 5). Scalariform and alternate pitting pattern is noticed on the walls of vessel elements. Xylem is composed of both libriform fibres and fibre-tracheids. These fibres are longer compared to those in healthy shoot (Table 5).

Vessels are surrounded by a few gelatinous fibres. The ray cells are noticed with phenolic accumulation (Fig. 22E). Pith region in some of the shoots is disrupted as a result of activity of insect borers. In response to the wounding, pith develops wound cambium resulting in the development of xylem towards the inner face of normal xylem ring. Neither hyphae nor conidia of the pathogen are encountered in these tissues.

### **3.2.8.0 Malformed Shoot : Histochemistry**

3.2.8.1 Starch : Epidermis, cortex, and pith parenchyma surrounding the gum-ducts, phloem parenchyma and xylem ray cells are almost free of starch grains (Fig. 22F).

3.2.8.2 Total proteins: Epidermis do not show any protein deposits. There are a few

protein bodies in outer and inner cortical parenchyma (Fig. 22G). The secretory or epithelial cells and the lumen of primary gum-resin duct stained positive for proteins (Fig. 22H) while secondary ducts lumen and epithelial cells are devoid of protein reserves. Phloem parenchyma, xylem ray cells and paratracheal parenchyma however, show more protein deposits.

**3.2.8.3 Total Lipids:** Lipid reserves are very few in the epidermal and cortical cells. More lipid bodies are found in primary duct lumen (Fig. 22I) phloem parenchyma, xylem ray cells (Fig. 23B) and pith cells.

**3.2.8.4 Succinic Dehydrogenase:** The enzyme activity is more in the epidermal and cortical cells (Fig. 23A). Primary duct epithelial cells and the parenchyma lying outside the duct do not show any reaction product. Some phloem and paratracheal parenchyma of vascular region show a strong reaction for the enzyme with granular precipitation (Fig. 23C). Xylem ray cells and pith parenchyma however, exhibit less reaction of the dehydrogenase.

**3.2.8.5 Peroxidase :** Epidermal cells do not show any activity of the enzyme. A few cortical cells exhibit a strong reaction product of the oxidase (Fig. 23D). The reaction product is mostly localised in the intercellular spaces of the cells. Phloem parenchyma (Fig. 23E), vessel elements at their radial walls, pith duct's epithelial cells and the outer parenchyma i.e., towards the inner cortex also are noticed with the peroxidase activity.

### **3.2.9.0 Malformed Leaves:**

The leaves are dorsiventral. The midrib epidermis is covered with a thick cuticle measuring 2.5-3.5  $\mu\text{m}$  in thickness (Fig. 23F). The cuticle often extends into the radial walls of the epidermal cells. A continuous band of sclerenchymatous fibres encircle the vascular bundles. There is a single gum-resin duct ring in the midrib. The lumen diameter of the gum-resin duct is less compared to the healthy ones (Table 5). The lumen diameter of vessel elements is less but their frequency is more compared to that of healthy leaves (Table 5). The vessel element walls are relatively thick and lignified (Fig. 23G). On the lower epidermis spores of *Alternaria* Sp. are found attached to the

stomata and in few instances these propagules are noticed even attached to the upper epidermis. Conidia or hyphal fragments of *F. moniliforme* are never found associated with the leaf tissue.

#### **3.2.10.0 Malformed Leaves : Histochemistry**

**3.2.10.1 Starch :** A few cells in ground tissue of midrib have starch deposits. There are no starch grains in the vascular cells. Starch grains are also noticed in the spongy parenchyma (Fig. 23H).

**3.2.10.2 Total Proteins :** The cells in the ground tissue of the mid rib have numerous protein bodies. Vascular tissue is free of protein bodies. Both the palisade and spongy parenchyma cells do show positive reaction for proteins (Fig. 24A).

**3.2.10.3 Total lipids :** Parenchyma of the midrib show accumulation of lipid bodies. Lipid bodies are also found in the ground parenchyma around the vascular tissue (Fig. 24B).

**3.2.10.4 Succinic Dehydrogenase :** The enzyme reaction is found associated with the palisade cells (Fig. 24C). Epithelial cells surrounding the gum-resin duct and vascular tissue also show enzyme activity. The enzyme activity is relatively less in spongy parenchyma.

**3.2.10.5 Peroxidase :** Epidermis and ground tissue exhibit little enzyme precipitation in the midrib while in the vascular tissue region, phloem parenchyma, vessel walls and a few ground parenchyma (Fig. 24D) located at distal end of vascular tissue show strong reaction of the oxidase. However the sclerenchymatous zone remains without any reaction product. In the lamina this enzyme is restricted to the epidermal cells of both the sides showing strong reaction (Fig. 24E).

#### **3.2.11.0 Healthy shoots :**

The cuticle covering the epidermis is thin ranging from 9.3-12.4  $\mu\text{m}$  in thickness. Cortical cell diameter ranges from 32-56  $\mu\text{m}$  and show phenolic contents. The outer

cortex contains 1-2 layers of sclerides which are relatively more lignified (Fig. 24F) than those of malformed ones. Perivascular fibres (Fig. 24G) are relatively thick and lignified. The lumen diameter of primary gum-resin ducts is relatively less than that in the malformed shoots (Table 5). Xylem consists of both solitary and multiple vessel elements. The paratracheal parenchyma do not show any deposits. Gelatinous fibres are distributed among the xylem parenchyma. Vessel lumen diameter is relatively more but their frequency is less compared to that of malformed shoots (Table 5). Xylem cylinder is mostly composed of primary xylem tracheary elements. Secondary xylem is less developed.

### **3.2.12.0 Healthy shoots : Histochemistry**

**3.2.12.1 Starch :** Epidermal cells have no starch deposits. Cortical parenchyma including the parenchyma surrounding the gum ducts, phloem parenchyma ray cells (Fig. 24H) and pith parenchyma have relatively more deposition of starch.

**3.2.12.2 Total proteins:** Cortical parenchyma, the parenchyma lying in the outer layers of the primary ducts (Fig. 25A) and the epithelial cells show more protein bodies compared to those of malformed ones while the primary and secondary duct lumen do not show any proteinaceous accumulation. Protein bodies are also absent in xylem ray cells and pith parenchyma.

**3.2.12.3 Total lipids :** Epidermal cells, cortical parenchyma, duct lumen and epithelial cells have less accumulation of lipid globules. Xylem ray cells are devoid of lipid deposition (Fig. 25B).

**3.2.12.4 Succinic Dehydrogenase :** Epidermal cells and immediate cortical parenchyma show little enzyme activity. Parenchyma and the epithelial cells surrounding the resin duct show some reaction product. Paratracheal parenchyma do not show any enzyme reaction (Fig. 25C).

**3.2.12.5 Peroxidase:** Epidermal cells do not show any enzyme activity. The cortical parenchyma (Fig. 25D) and parenchyma around gum ducts are noticed with little

reaction product. Phloem parenchyma, xylary fibres show more peroxidase activity than those of malformed ones. Cell walls of vessel elements exhibit less activity compared to that of malformed ones.

#### **3.2.13.0 Healthy leaves :**

Cuticle measuring 2.0-2.5  $\mu\text{m}$  thickness (Fig. 25E) covers the epidermis on both the sides of leaf. The sclerenchymatous perivascular fibres form a continuous band over the gum-resin duct. The gum-resin duct lumen diameter is more compared to that of malformed ones (Table 5). The vessel element walls are relatively thin. The structure of lamina remains similar to that of malformed leaf.

#### **3.2.14.0 Healthy Leaves : Histochemistry**

**3.2.14.1 Starch:** Starch deposition is more in vascular cells and mesophyll cells. Spongy parenchyma cells deposit relatively more starch grains (Fig. 25F).

**3.2.14.2 Total Proteins:** Epidermal cells and a few ground parenchyma of midrib have relatively more protein bodies. The secretory and the parenchyma cells in outer cortex of both healthy and malformed leaves do not show any protein deposits. The palisade and spongy parenchyma have relatively less deposition of protein bodies.

**3.2.14.3 Total lipids :** Lipid bodies are not found in the midrib and the lamina of leaves.

**3.2.14.4 Succinic Dehydrogenase:** Epidermal cells show less enzyme reaction. In the ground tissue, the epithelial cells of gum ducts show scanty reaction product. The enzyme activity in xylem, palisade and spongy tissue is similar to that noticed in malformed leaves.

**3.2.14.5 Peroxidase:** Epidermis and ground parenchyma of midrib show less peroxidase activity. Vessel elements and phloem parenchyma show little enzyme activity compared to those of malformed leaves (Fig. 25G). In the lamina, the enzyme reaction is associated with upper epidermal cells (Fig. 25H).

### 3.3.0 Ultrastructural Observations :

#### 3.3.1 Transmission electron microscopy :

Ultrathin sections of resin embedded young buds, mature anthers and ovary have been observed under transmission electron microscope. Transverse and obliquely cut fragments of *F. moniliforme* hyphae are frequently observed in between the whorls of the sepals and petals and close to the anther lobe in young buds (Fig. 26A).

Sections passing through young anthers reveal the ultrastructure of tapetal and microspore mother cells. Both the cells are densely cytoplasmic with many small vacuoles (Fig. 26B,C). The cytoplasm in both these cells is often appear plasmolysed. Tapetal cells are characterised by darkly stained cytoplasm containing smooth vacuolated ER (Fig. 26D). The cytoplasm also exhibits vacuoles with electron dense bodies and membranous contents (Fig. 26E,F). Lipid globules of different sizes and electron dense bodies appearing as globular and spindle-shaped are frequently found in the cytoplasm of microspore mother cells (Fig. 26G). The cell walls are thin and sometimes appear wavy in nature.

Transverse and obliquely cut fragments of hyphae are noticed close to the basal epidermis of the mature anther lobes (Fig. 26H). The epidermal cells are covered with thick serrated cuticle (Fig. 26H). The cells have plasmolysed electron dense cytoplasm (Fig. 27A). The parenchyma cells of anther close to the basal epidermal cells and around the connective show distinct intracellular hyphae (Fig. 27C,D). The cell containing hyphal structure have cell walls which are electron dense (Fig. 27B). The tracheary elements of the connective are filled with electron dense granular contents in their lumen (Fig. 27E) The parenchyma cells next to the tracheary elements show electron dense material filled with a mass of electron dense cytoplasm (Fig. 27F). These cells have usually thick irregular cell walls. The endothelial cells also have such cell walls. The cells around the connective have quite thick walls with electron dense material in their cytoplasm.

The stylar transmitting tissue at the site of infection shows irregularly shaped cells with electron dense material. These cells have usually thick walls enclosing dark

cytoplasmic contents either partially or completely occupying the cell lumen (Fig. 28B). The dark mass of cytoplasm appears irregular in shape occurring in the centre of cells or along cell walls. Some of the stylar transmitting cells of the ovary possess large lipid bodies, numerous small vacuoles and electron dense contents (Fig. 28A). Intercellular spaces are distinct among the stylar transmitting tissue (Fig. 28C). The inner most layers of ovary wall surrounding the ovular chamber show irregularly flattened cells with thickened walls. These cells are also either partially or completely filled with electron dense contents (Fig. 28D). The vascular traces in the ovary wall are distinct surrounded by cells containing electron dense material (Fig. 28E).

The outermost cell layers of ovule are filled with electron dense contents. The cell walls appear wavy and irregularly thickened. Irregularly shaped vacuoles are prominent in these cells. In some of the cells the vacuoles are large occupying much of the cell lumen reducing the dense contents to the periphery of the cell walls. Conidia - like structures are often found closely attached to the surface of the ovule (Fig. 28F,G). These structures have thick walls enclosing electron dense cytoplasm. Some of the ovule cells are flattened and filled with dark contents and small vacuoles. In a few instances intracellular hyphal fragments are also noticed in these cells (Fig. 28H).

### 3.3.2 Scanning Electron microscopy :

Sepals, anthers and ovary from mature flowers of malformed panicles have been observed under scanning electron microscope. Hyphal filaments of *Fusarium moniliforme* in the form of mat are found attached on the ventral surface of the sepals (Fig. 29A). The anthers from flowers of malformed panicle have no distinct grooves on the epidermal surface (Fig. 29C) while in the anther of healthy flowers such grooves are distinct (Fig. 29B). Hyphal filaments of *Fusarium* are often noticed attached to the surface of malformed anther wall. The filament of anther is usually basifixed and the point of attachment appears weak wherein only the tip of the filament is loosely embedded in the groove formed by the anther lobes.

The basal portion of the anther lobe where the filament is attached is often noticed with a tuft of coiled hyphal filaments of the pathogen (Fig. 29D-F). In a few instances the pathogen is also noticed inbetween the two anther lobes (Fig. 29G). The

anther locule contains a few oval-elliptical pollen grains. Some of these appear disorganised (Fig. 29H). The hyphal filaments of the pathogen found between the two lobes of the malformed anther are long, slender and appear closely arranged. The ovary of the healthy flowers is often found with waxy sheath-like endocarp. Such sheath-like endocarp is absent in malformed ovary. A few hyphal filaments are found attached to the outer surface of the ovule.

Table 1: Size variation of essential and non-essential organs in Malformed (M) and Health (H) flowers in *M. indica* var. Rajapuri

	Sepals	Petals	Staminodes	Anthers	Pollen grains	Ovary	Glandular Disc.	Peduncle (Thickness)	Pedicel (Thickness)
M	3.9 mm ±0.40	3.9 mm ±0.50	0.85 mm ±0.10	2.25 mm ±0.35	26.76 µm ±1.035	2.15 mm ±0.35	3.28 mm ±0.30	3.05 mm ±0.67	1.06 mm ±0.16
H	2.7 mm ±0.25	3.6 mm ±0.2	0.56 mm ±0.05	2.07 mm ±0.17	27.52 µm ±1.71	1.1 mm ±0.20	2.15 mm ±0.20	1.89 mm ±0.44	0.61 mm ±0.18

Table 2 . Percentage Area (PA), Frequency (FR) and Mean lumen diameter (LD) of gum-resin ducts in 1 sq.mm of pith in shoot terminal buds of *M. indica* L. var. Rajapuri collected at monthly intervals for one year.

	PA	FR	LD ( $\mu\text{m}$ )
Jan	15.4	3.4 $\pm$ 2.6	321
Feb	3.4	2.9 $\pm$ 1.4	687
Mar	16.0	3.7 $\pm$ 1.5	176
Apr	8.1	3.5 $\pm$ 1.5	153
May	2.5	1.8 $\pm$ 0.9	99
Jun	3.2	0.8 $\pm$ 0.8	90
Jul	6.4	1.8 $\pm$ 1.1	126
Aug	4.4	2.5 $\pm$ 1.4	216
Sept	6.4	2.2 $\pm$ 1.1	117
Oct	2.8	2.7 $\pm$ 1.6	111
Nov	15.7	3.5 $\pm$ 1.2	203
Dec	8.1	2.5 $\pm$ 1.4	178

Table 3: Anatomical variations in Peduncle and Mature Pedicel of Malformed (M) and Healthy (H) Panicles of *M. indica* var. Rajapuri

	Peduncle		Pedicel	
	M	H	M	H
Cuticle thickness ( $\mu\text{m}$ )	7.2 $\pm 1.5$	1.3 $\pm 0.5$	1.8 $\pm 0.7$	1.2 $\pm 0.6$
Cortical cells diameter ( $\mu\text{m}$ )	39.6 $\pm 6.8$	26.4 $\pm 2.2$	35.3 $\pm 5.7$	24.8 $\pm 2.7$
Pith cell diameter ( $\mu\text{m}$ )	51.3 $\pm 13.9$	39.6 $\pm 7.2$	34.8 $\pm 4.0$	25.6 $\pm 6.4$
Phloem duct lumen diameter ( $\mu\text{m}$ )	62 $\pm 11.0$	104 $\pm 25.5$	85 $\pm 20.0$	51 $\pm 7.0$
Vessel frequency (in 1 $\text{mm}^2$ )	30 $\pm 4.7$	20 $\pm 2.0$	36 $\pm 4.0$	23 $\pm 2.0$
Vessel element length ( $\mu\text{m}$ )	141 $\pm 6.0$	110 $\pm 4.5$	-	-
Vessel element width ( $\mu\text{m}$ )	58 $\pm 3.0$	40 $\pm 1.0$	-	-

**Table 4 : Dimensional changes of buds, flowers and floral parts between malformed and healthy panicles of *M. indica* var. Rajapuri**

	Malformed	Healthy
Young buds (Mean size)	0.72 mm ±0.02	0.60 mm ±0.02
Mature buds (Mean size)	3 mm ±0.23	1.55 mm ±0.18
Open flowers (Mean size)	4.25 mm ±0.46	3.57 mm ±0.25
Anther cuticle (mean thickness)	11.36 m ±3.52	3.52m ±1.28

Table 5 : Showing the dimensional details of vessels, fibres and gum-resin ducts in the shoot and leaf of *M. indica* var. Rajapuri

	Shoot		Leaf	
	Malformed	Healthy	Malformed	Healthy
Vessel lumen diameter ( $\mu\text{m}$ )	58.7 $\pm 11.4$	60.0 $\pm 14.3$	23.3 $\pm 4.0$	34.3 5.6
Vessel frequency (in 1 sq mm)	6.4 1.7	4.4 1.4	13.1 4.7	12.7 $\pm 2.5$
Gum resin duct lumen diameter ( $\mu\text{m}$ )	88.04 $\pm 14.1$	77.84 $\pm 10.2$	130.5 $\pm 45.0$	188.3 $\pm 77.5$
Length of libriform fibres ( $\mu\text{m}$ )	629 $\pm 210$	270 $\pm 44$	-	-
Length of fibre tracheids ( $\mu\text{m}$ )	416 $\pm 70$	238 $\pm 35$	-	-

Fig. 1. Map showing percentage occurrence of mango malformation in and around Baroda.

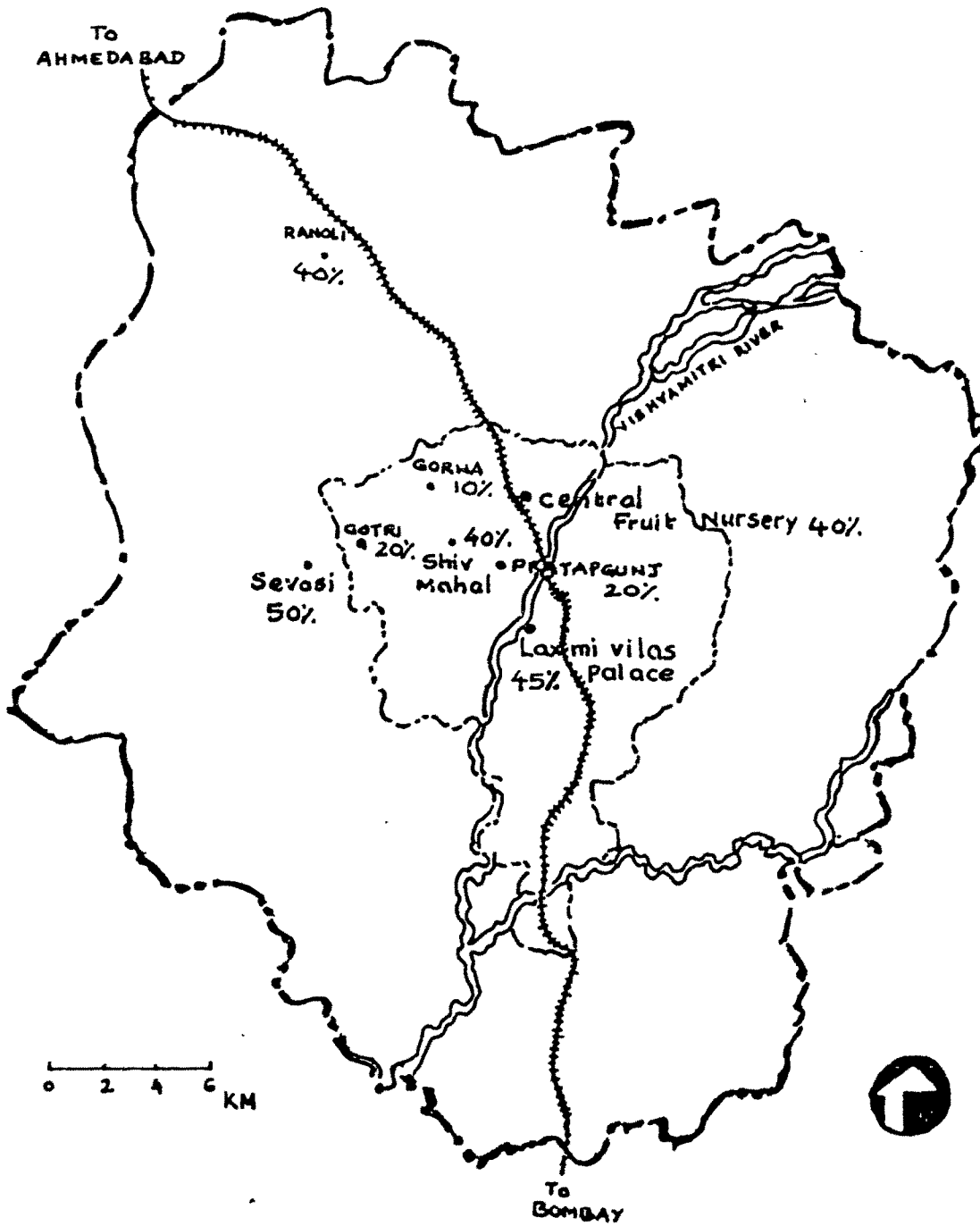


FIG.1

- Fig. 2. A Photograph showing a healthy panicle of mango cultivar Rajapuri
- B Photograph showing a malformed panicle of mango cultivar.Rajapuri.



FIG.2

Fig. 3. Histogram showing percentage occurrence of male and hermaphrodite flowers of eight cultivars of mango.

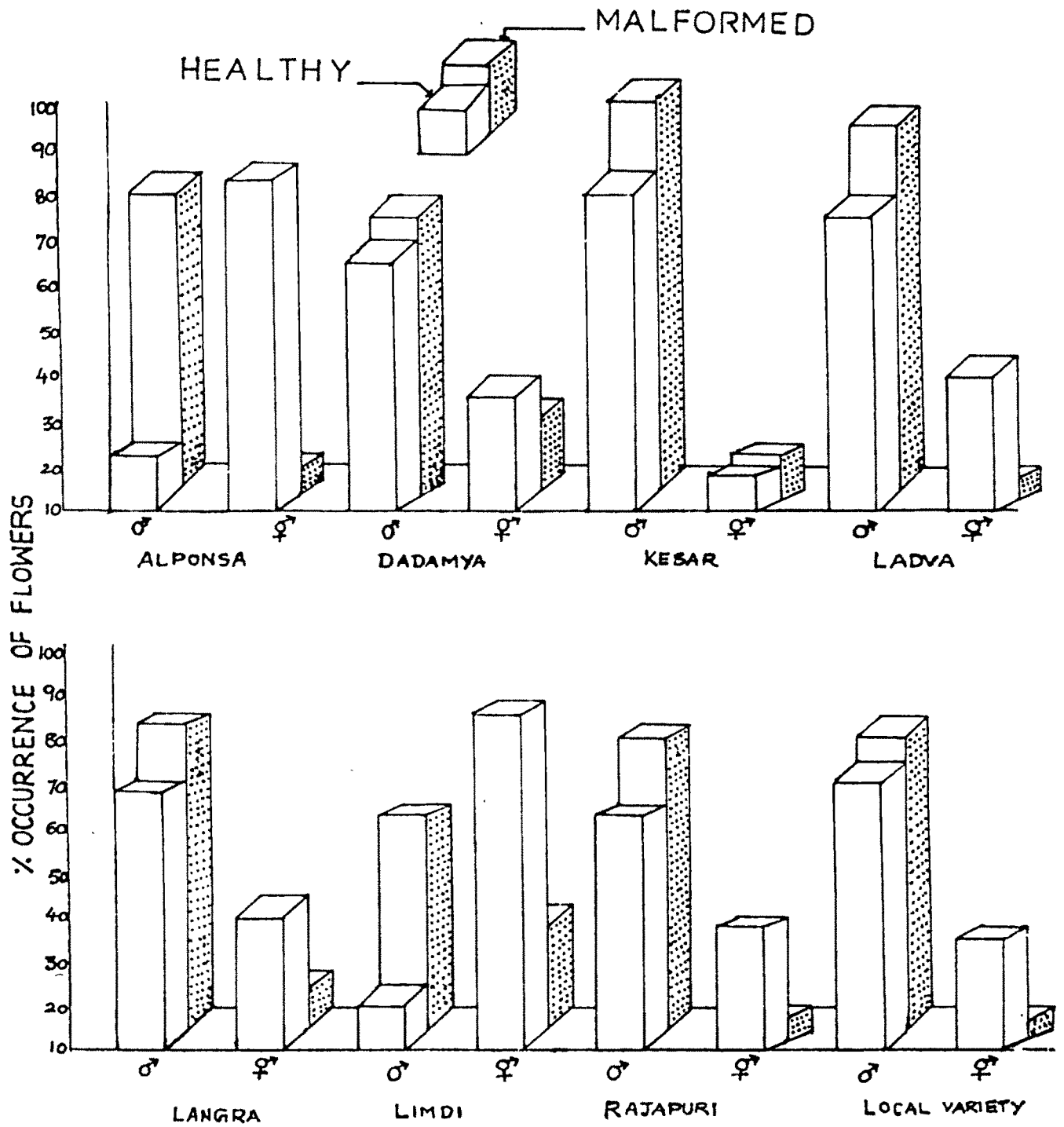


FIG.3

- Fig. 4. A Hermaphrodite flower from healthy panicle of mango cultivar Rajapuri. X10
- B Hermaphrodite flower from malformed panicle of mango cultivar Rajapuri. Note the enlarged organs of the flower. X8

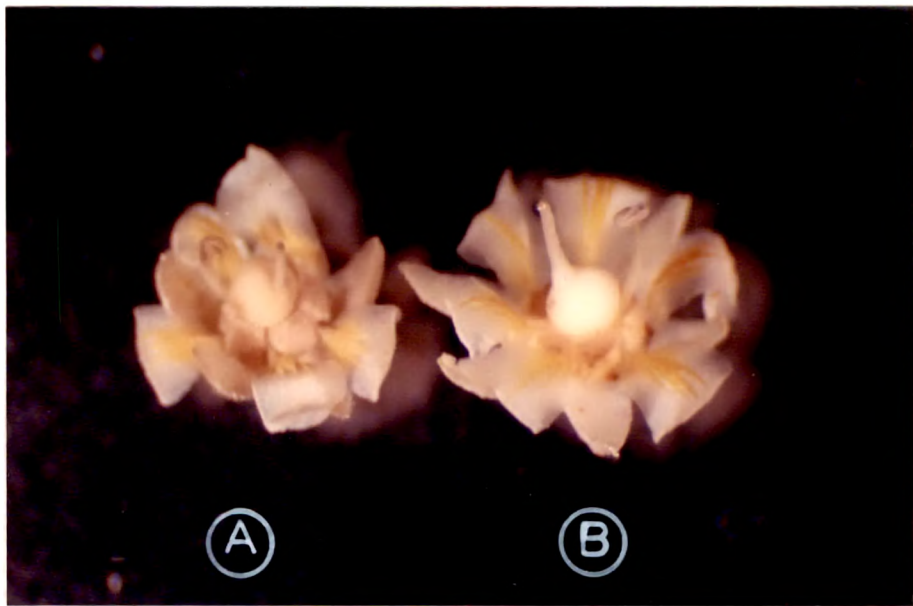


FIG.4

- Fig. 5. A Terminal bud of mango cultivar Rajapuri during floral season (January) with a few open small bud scales X3
- B Opening of terminal bud in mango cultivar Rajapuri during floral season (January) with large leafy bud scales. X4
- C Remnants of vegetative malformed twig of Rajapuri cultivar showing vegetative malformed shoots and young malformed panicle in the bearing season.



FIG.5

- Fig. 6. A Light malformed panicle at a young phase of development at the axil of tender leaves of Rajapuri variety.
- B Light malformed panicle of Rajapuri variety at a mature phase at the axil of maturing leaves.



FIG.6

- Fig. 7. A Symptoms of vegetative malformation showing stunted buds at apex as well as axillary positions of leaves of cultivar Rajapuri.
- B Typical vegetative malformed twig with dwarf shoots of cultivar Rajapuri.



FIG. 7

- Fig. 8. A Tip portion of shoot bud from vegetative malformed twig of Rajapuri variety. Note the ring like opening of the bud tip (arrow head). X112
- B Close view of the terminal bud tip. X282
- C Young mite showing dark specks (arrow) of *Fusarium* mycelium. X250
- D An adult mite showing spores of *Fusarium* and mycelial specks attacked to its body parts. X145
- E Enlarged view of lateral side of an adult mite with microconidia (arrows) attached to its body. X400

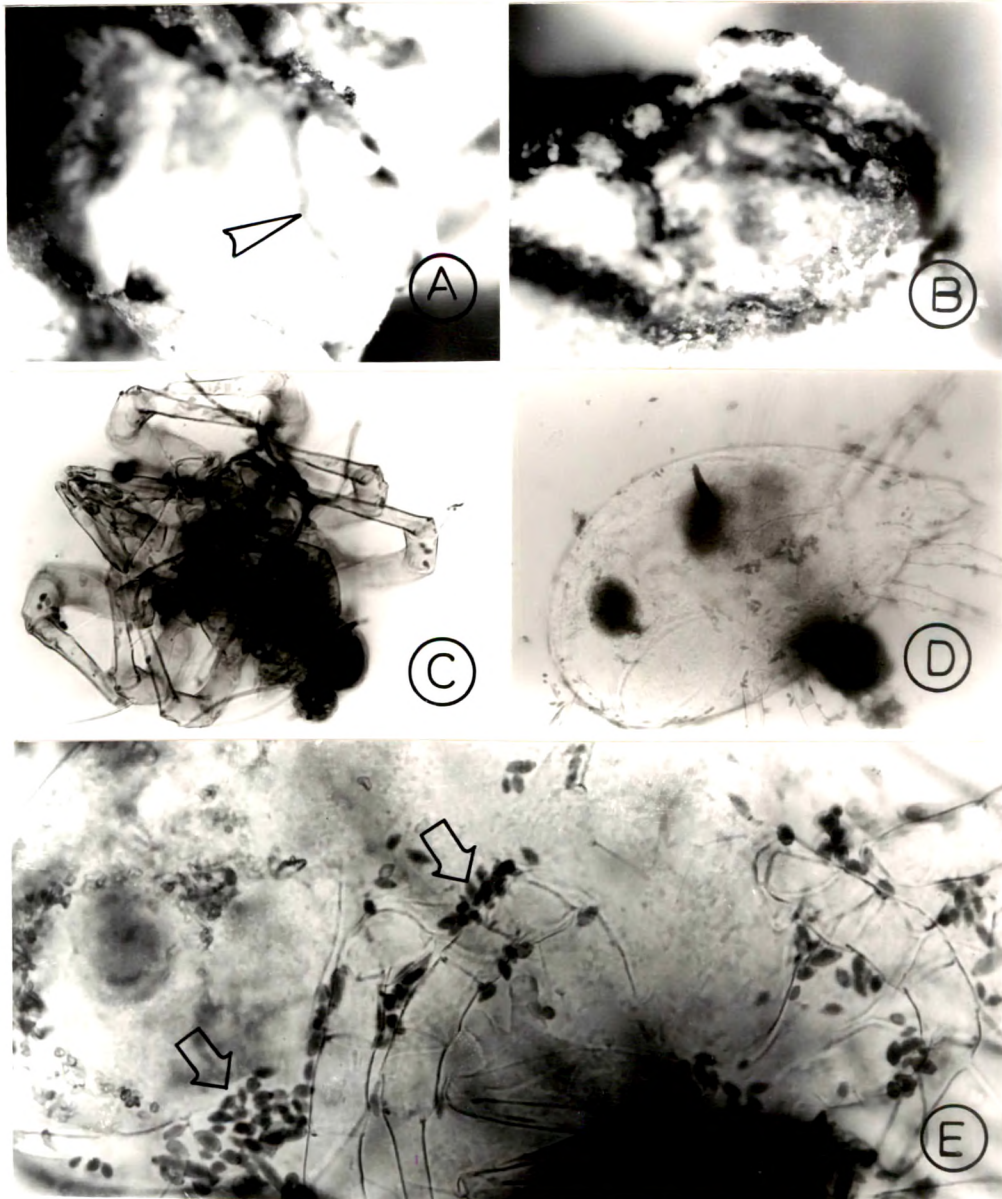


FIG. 8

- Fig. 9. Longitudinal sections of terminal buds of mango cultivar Rajapuri.
- A Floral bud showing elongated axis with axillary bud meristems in winter. X202
  - B Hyphal filaments noticed in between young bract primordia in floral apex (arrow). X112
  - C Enlarged portion of Fig. B showing tuft of mycelium close to the bud meristem (arrow). X647
  - D Hyphal strands of *Fusarium* (arrow) attached to the bract primordia of floral meristem in winter. X164
  - E Enlarged portion of Fig. D showing conidiophores of *Fusarium* (arrow). X625
  - F A leaf primordium showing dark contents in mesophyll in March. Also note hyphal mat (arrow head) attached to it. X164
  - G Probable entry of hyphal filament (arrow) through the base of leaf primordium next to the bud meristem. X250
  - H Intercellular proliferation of hyphae in shoot (arrow). X800

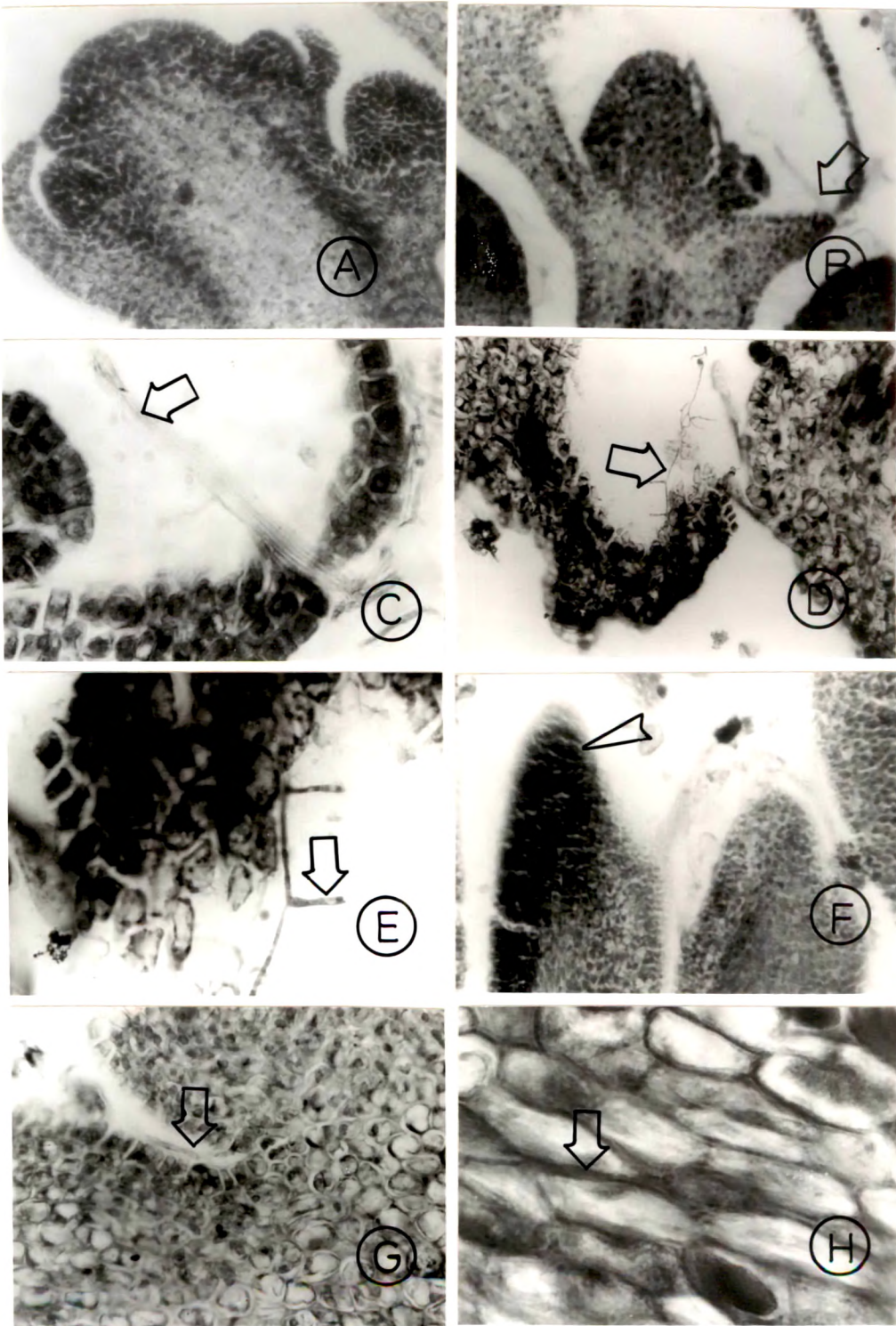


FIG.9

- Fig.10. A-H Longitudinal sections of terminal buds of mango cultivar Rajapuri.
- A The gum-resin duct lumen in the shoot showing deposition of secretory material in March (arrow). X200
  - B Shoot apex in May showing darkly stained tunica (arrow) and a few lightly stained cells in the corpus (arrow head). X202
  - C A duct showing no secretory content in summer (arrow). X200
  - D Spores of *Alternaria* (arrow) and insect remains segmented (arrow head) in between two adjacent leaf primordia. X202
  - E Remains of insects possibly mites (arrow) and *Alternaria* spores in close association with leaf primordia of apices during monsoon. X290
  - F Infected apical meristem showing disrupted tunica layer in November. Note the accumulation of phenolic contents at the site of infection (arrow). X320
  - G A portion of shoot apex showing accumulation of starch (arrow) in December. X202
  - H Relatively more deposition of starch in the shoot cells (arrow) of apices in January. X320

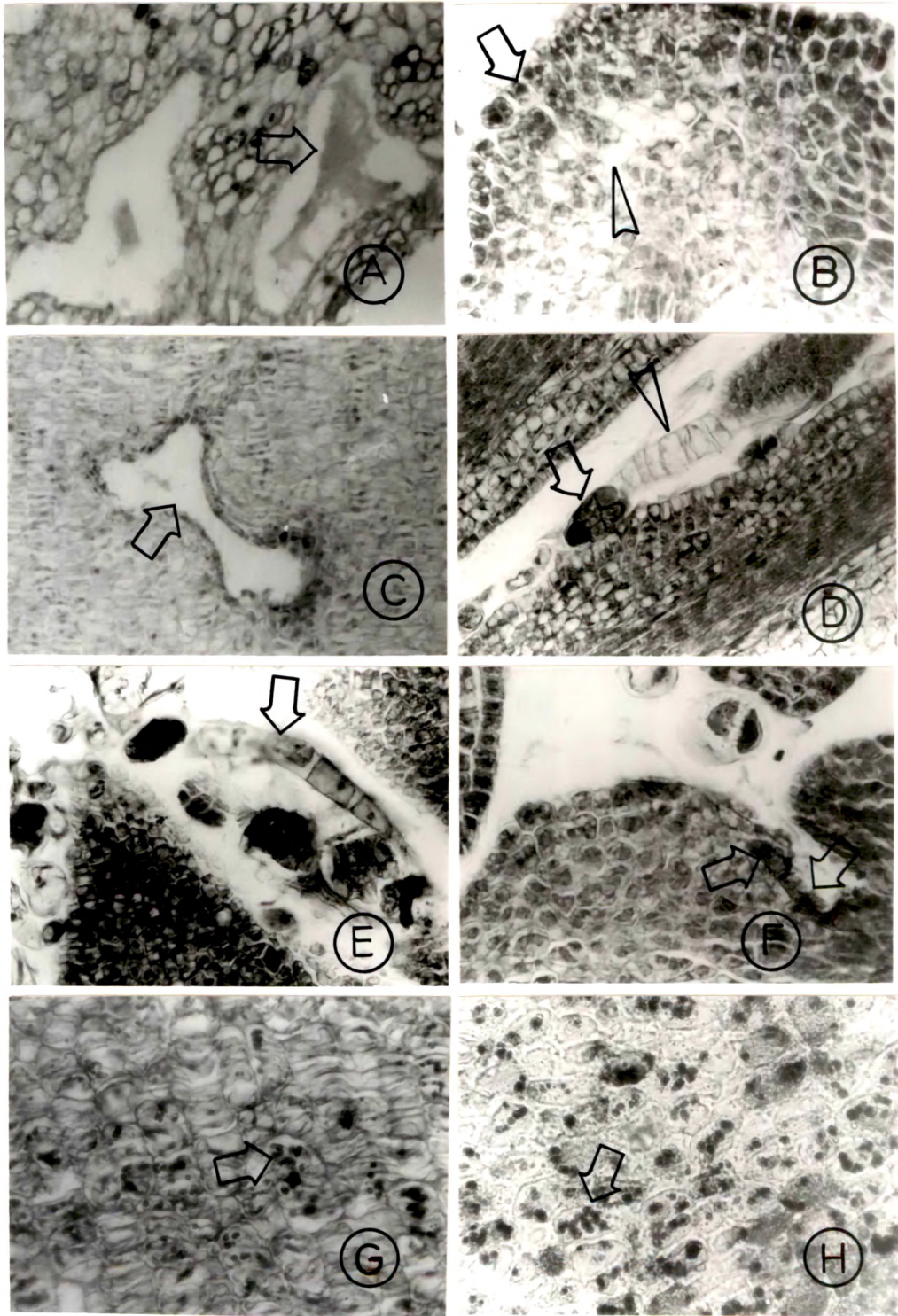
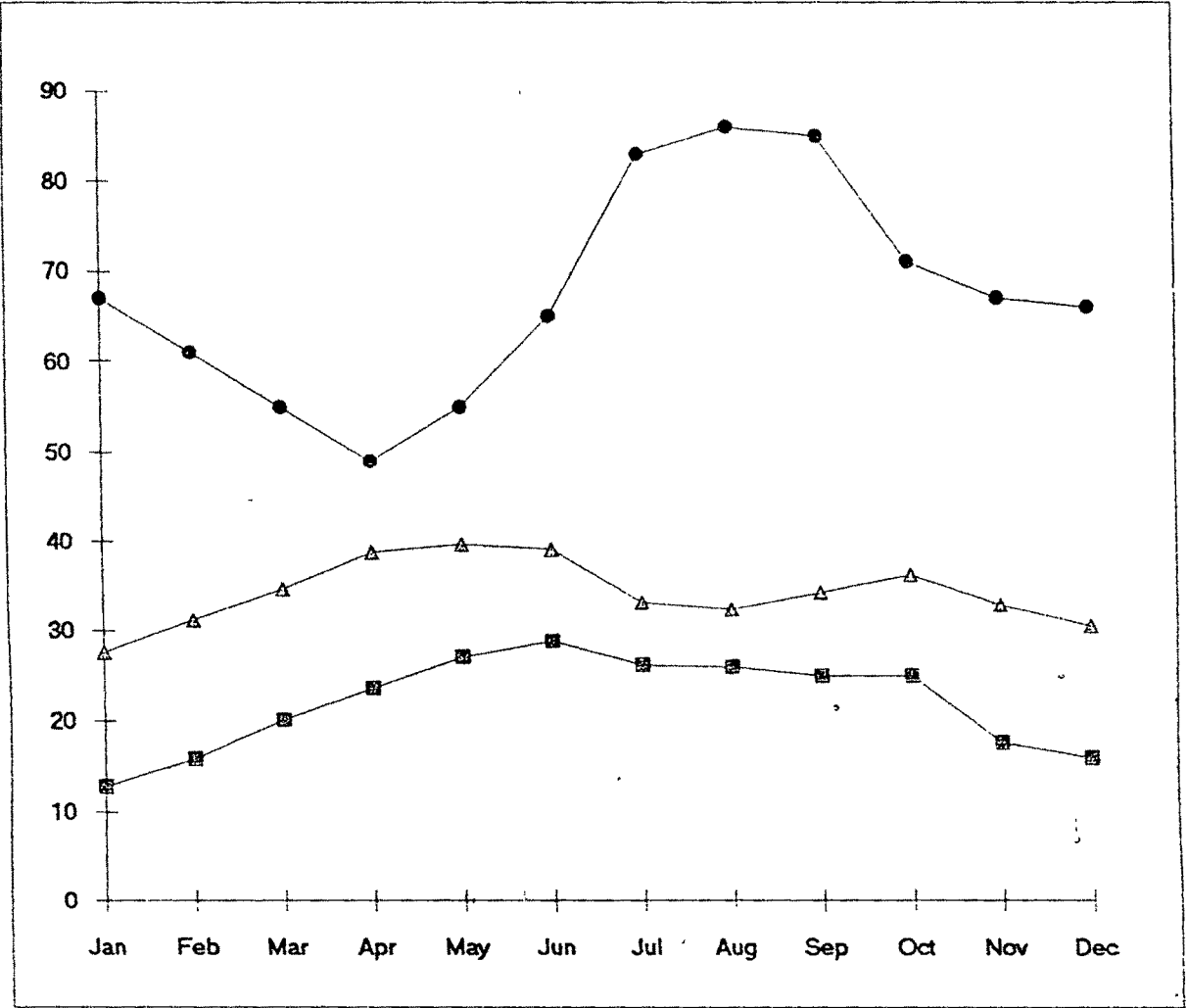


FIG.10

Fig.11. Graph showing meteorological data viz. minimum and maximum temperatures and mean relative humidity in Vadodara during the year (1995-96).



■ - Minimum Temperature °C  
 ▲ - Maximum Temperature °C  
 ● - Mean Relative Humidity (%)

FIG. 11

Fig.12. A-H Longitudinal sections of mango shoot buds and malformed panicle axis of cultivar Rajapuri.

- A The pith duct of shoot in March showing proteinaceous resin (arrow). X725
- B Parenchyma cells below corpus zone in the shoot showing protein bodies (arrow). X700
- C Lipid bodies in the tunica (arrow) and corpus layers (arrow head) of shoot apex in March. X700
- D Pith cells of shoot in November with phenolic contents (arrow) and lipid bodies (arrow head). X700
- E Epidermal cells of peduncle showing thick cuticle (arrow). Arrow head indicates the extension of cuticle on the radial walls. X700
- F Intra (arrow) and intercellular (arrow head) hyphal filament in the cortex of peduncle. X252
- G Thick and lignified perivascular fibres (arrows) encircling the primary gum resin ducts (r) in the cortex of the peduncle. X164
- H A gum-resin duct of peduncle with epithelial cells (arrows) free of secretory material. X725

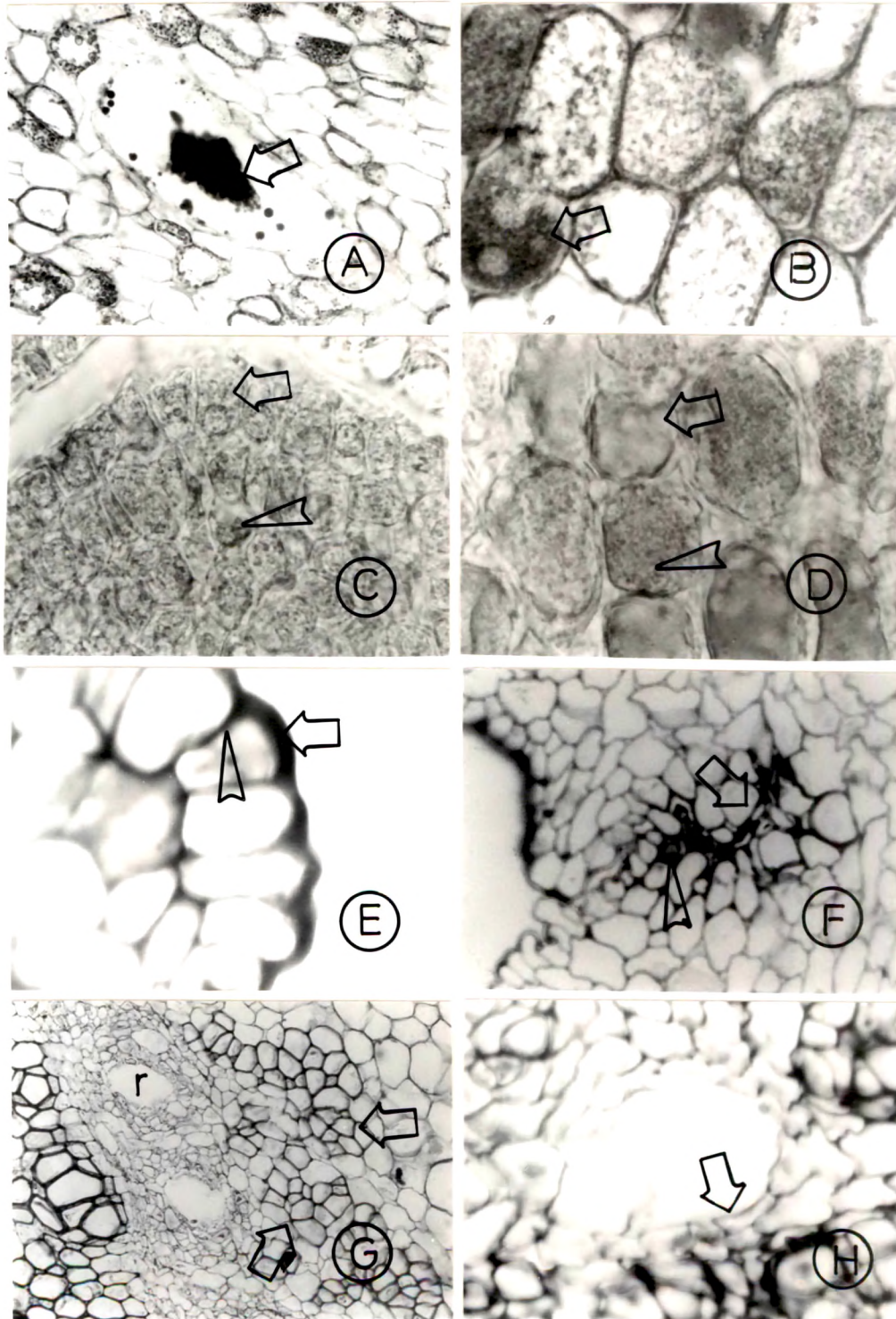


FIG.12

Fig.13. A-H Longitudinal sections of mango buds from malformed panicles of variety Rajapuri.

- A Mature pedicel showing confluent gum-resin ducts (arrows). X189
- B Resin embedded semithin section showing a pile of microconidia of *Fusarium moniliforme* (arrows) in between sepals and petals of young buds. X546
- C Necrotic sepals (arrow) of young buds indicating the pathogenic interaction. X108
- D Young monoecious bud showing close association of hyphal filaments of *Fusarium* with anthers (arrow) and ovary (arrow head). X260
- E Mature anther showing attachment of thick darkly stained mycelial mat of *Fusarium* in the basal groove of anther lobes (arrows). X170
- F Mature anther with thick mat of *Fusarium* in close association with the connective (arrow). X92
- G A thick mat of *Fusarium* (arrow) at the basal groove of anther lobes. X258
- H Basal portion of mature anther showing disorganised portion of filament (arrow head) and mycelial mat attached to the cells in the groove (arrow). X216

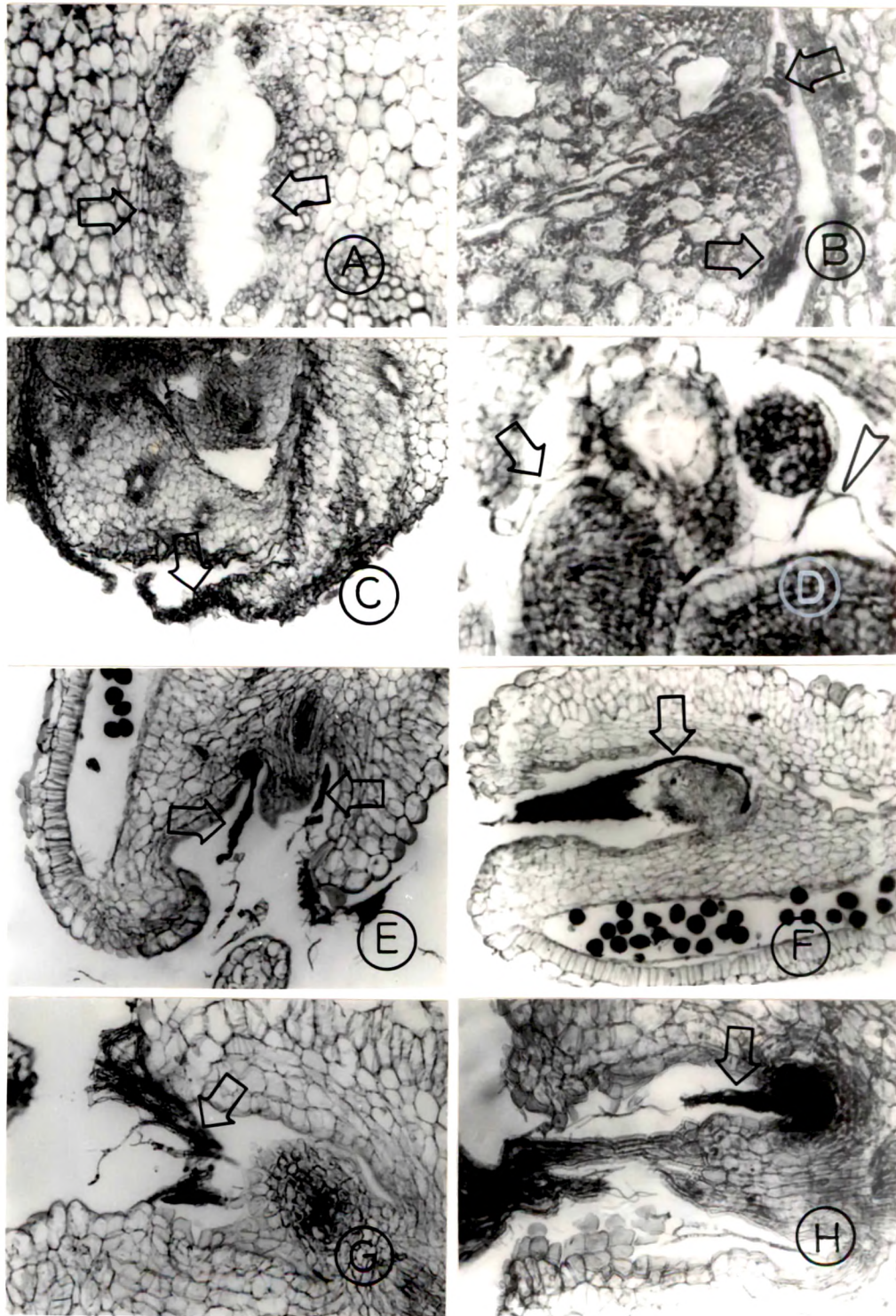


FIG.13

Fig.14. A-H Longitudinal sections of mango flowers of var. Rajapuri (A-D and H) and Dadamio (E-G) from malformed panicles.

- A Part of anther showing hyphal filament (arrow) inside the locule as seen under fluorescence light. X264
- B An anther locule showing hyphal filaments and mat of *Fusarium moniliforme* (arrow). X270
- C A thick mat (arrows) of *Fusarium* in between two lobes of the anther. X170
- D Mature anther locule showing pollen grains and disorganised tapetal layer (arrow head). X428
- E One of the anther lobes showing association of fungal hyphae with the pollen grains. X116
- F Part of the anther locule with fungus in association with pollen grains. Note the tuft of mycelium at anther-filament attachment (arrow head). X151
- G Pollen grains with attached fungal hyphae (arrows) in the anther locule. X500
- H Single pollen grain showing intimate association with fusarial mat (arrow). Note the disorganised wall of the pollen (arrow head). X510

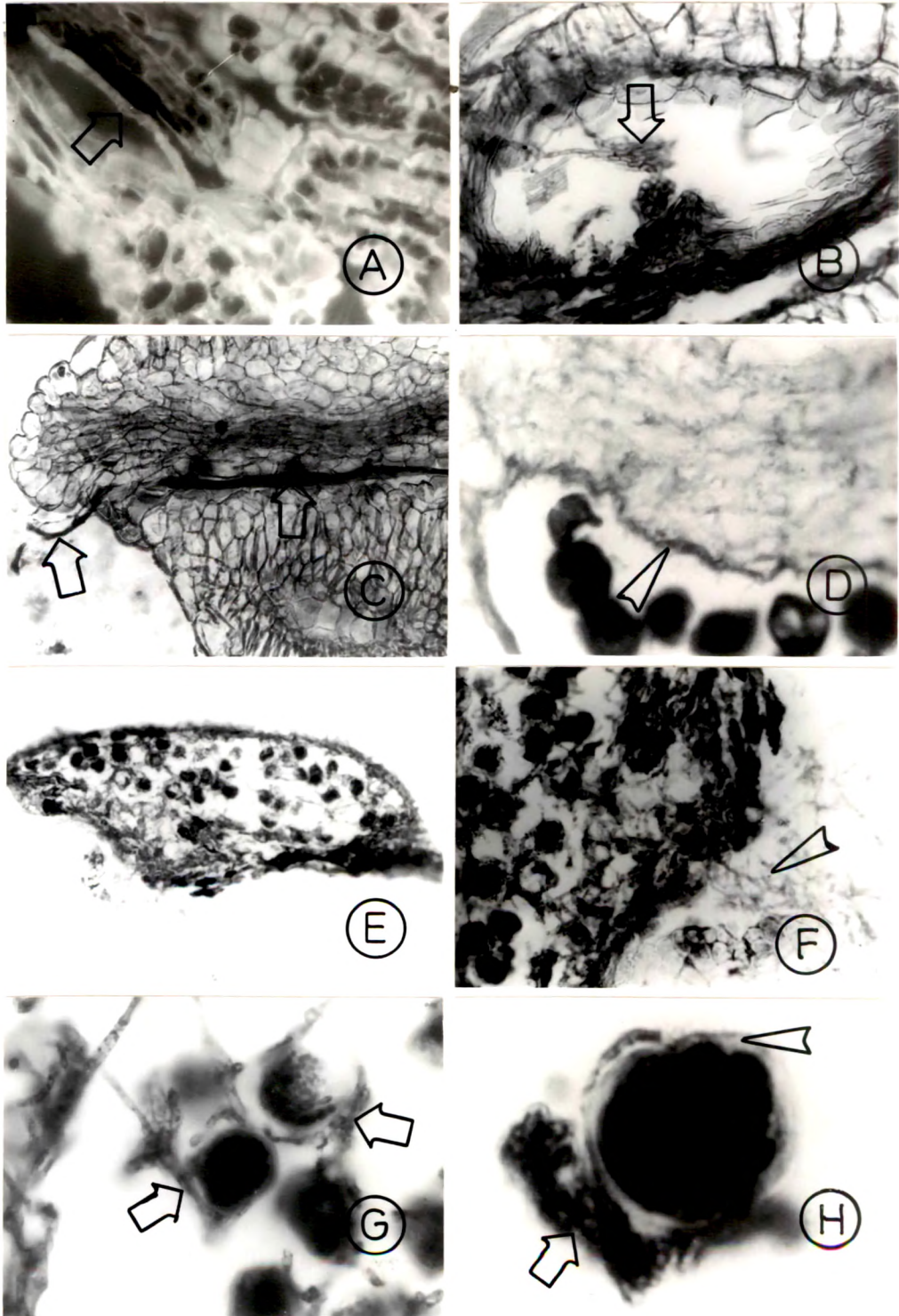


FIG.14

Fig.15. Longitudinal sections of anther and ovary from malformed and healthy panicles

- A Anther locule of variety Dadamio with aborted pollen grains (arrow) and necrotic cell walls of pollen. X240
- B Pathogen free anther locule showing pollen grains with dense cytoplasm in the healthy flower of variety Dadamio. X270
- C Basal portion of anthers from a healthy flower of variety Rajapuri showing *Fusarium* free basal groove and intact filament (arrow). X92
- D An entire ovary from a malformed flower of variety Kesar showing necrotic style (arrow) and aborted ovule (arrow head). X20
- E Bifid stigmatic groove showing lesion (arrow) towards the transmitting tissue of the style of var. Kesar. X132
- F Fusarial mat (arrow) at the opening of the bifid stigma. Note the lesion in the transmitting tissue (arrow head). X132

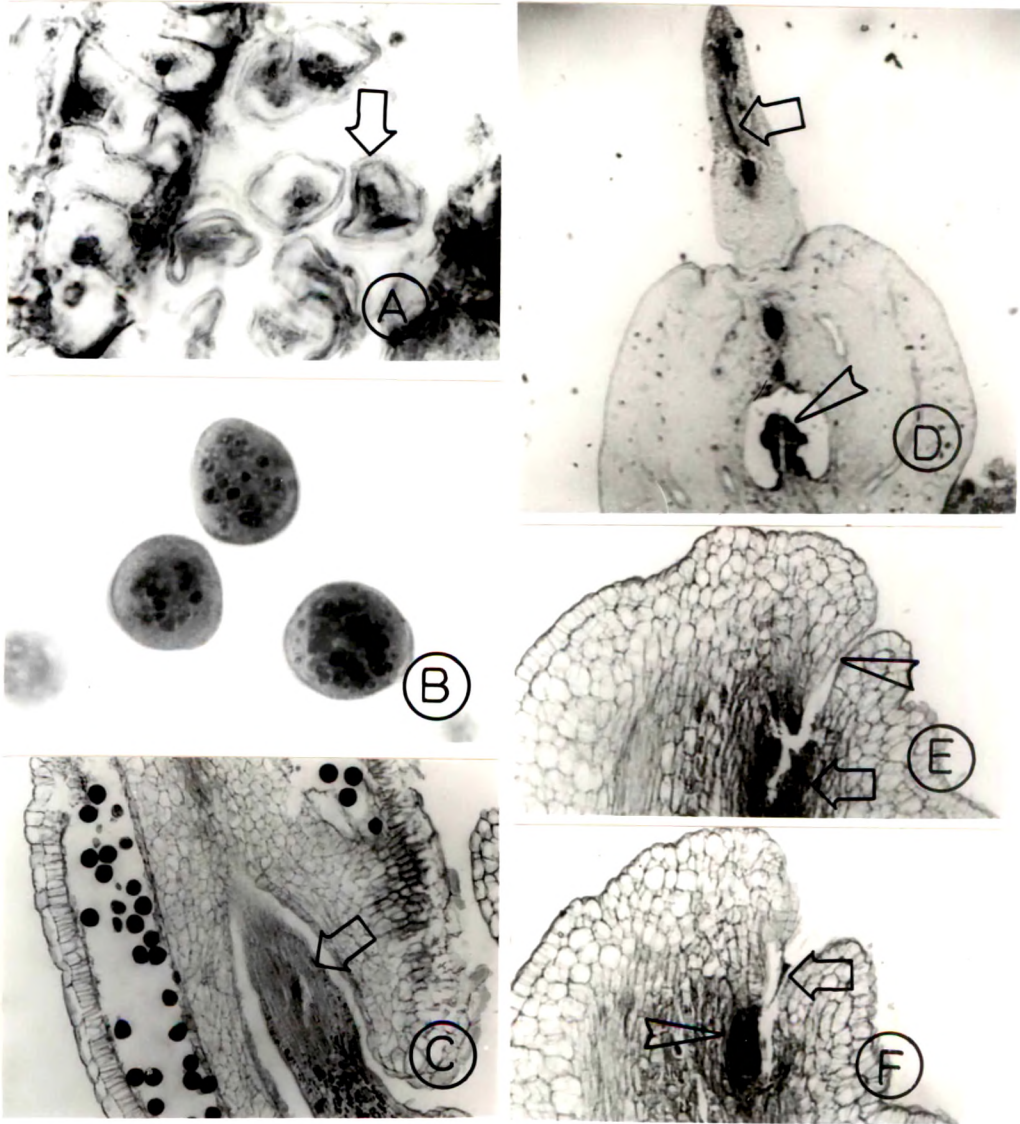


FIG.15

**Fig.16.** Longitudinal sections of style and ovary wall of malformed panicles.

- A** Lesions along the stylar transmitting tissue starting from stigma till the ovular chamber (arrows) indicating a probable site of entry of the pathogen into the ovary of var. Kesar. X403
- B** Stylar canal formed by the disorganisation of transmitting tissue of var. Rajapuri showing fusarial mat (arrow). Note the accumulation of phenolic contents in the cells on either side of the canal (arrow head). X214
- C** Semithin section showing fusarial mat (arrow) in the stylar canal opening into the ovular chambers in var. Rajapuri. X334
- D** A distinct lesion (arrow) across the ovary wall of var. Kesar indicating the probable site of entry of the pathogen. X108

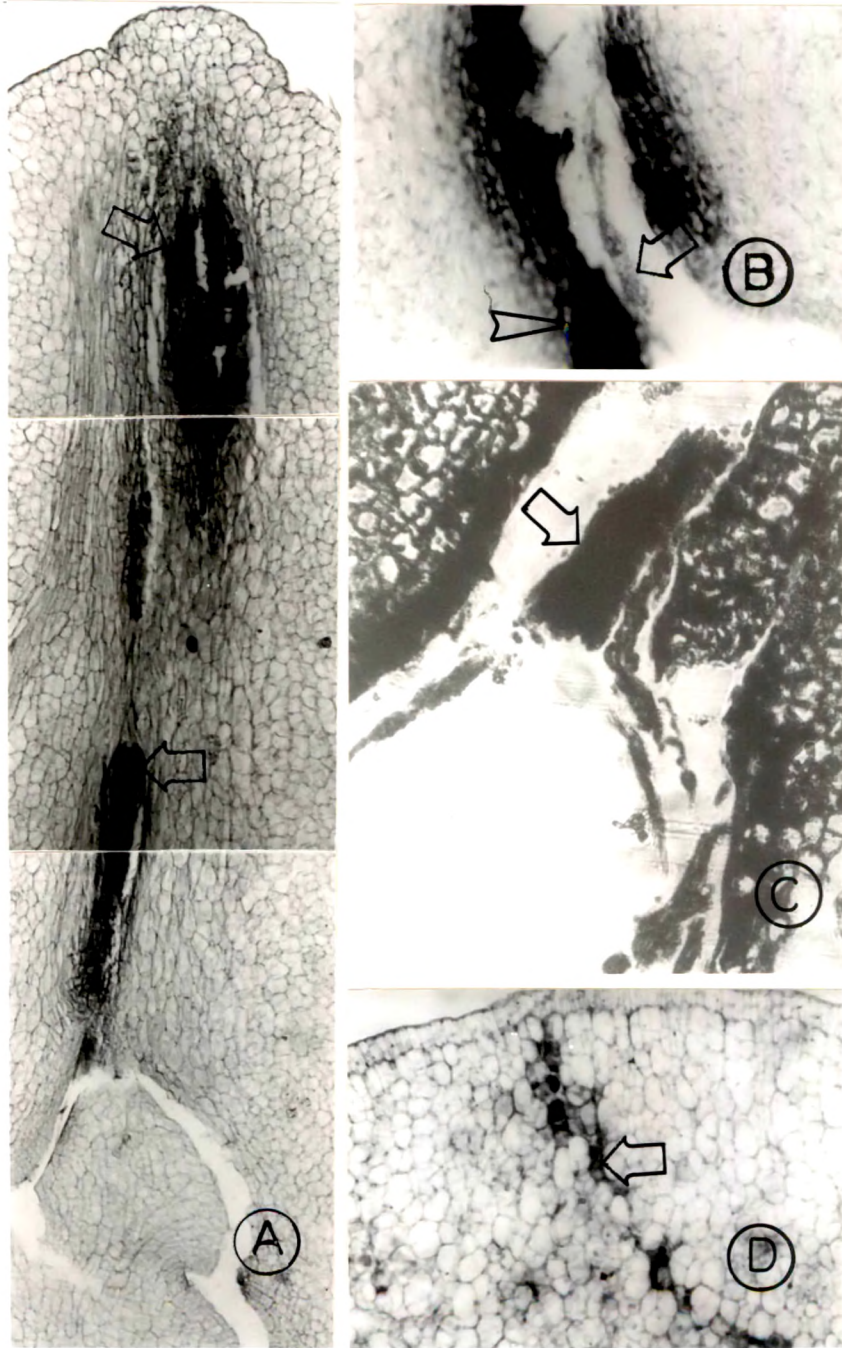


FIG.16

Fig.17. Longitudinal sections of malformed ovary (A-H) and gland from malformed flower (I).

- A Micropylar end of ovule with filaments of *Fusarium moniliforme* attached to it (arrow) in Rajapuri cultivar. X250
- B Hyphal filament (arrow) of *Fusarium* attached to the ovule of variety Rajapuri at the micropylar end. Also note the chlamydospore like globose structure near to it (arrow head). X625
- C Chlamydospore-like structures (arrow) in the filament of *Fusarium* near the ovule (ov) of variety Rajapuri. X625
- D Intracellular mycelium (arrows) in the ovary wall of var. Kesar. X575
- E Ovular chamber of variety Kesar with aborted irregularly shaped ovule containing dark contents (arrow head). Note the mycelium of *Fusarium* projecting from the inner layers of ovary wall (arrow). X96
- F A portion magnified from Fig. E showing the projecting mycelium of *Fusarium* from the inner layer of ovary wall (arrow). X625
- G An aborted irregularly shaped ovule of Kesar variety with associated mycelium (arrow head). X183
- H A portion magnified from Fig. G showing mycelial fragments of *Fusarium* (arrow) projecting from the aborted ovule. X675
- I Ovular gland of variety Rajapuri showing necrotic region (arrows) in columnar cells with phenolic accumulation and associated mycelium (arrow head) of the pathogen. X108

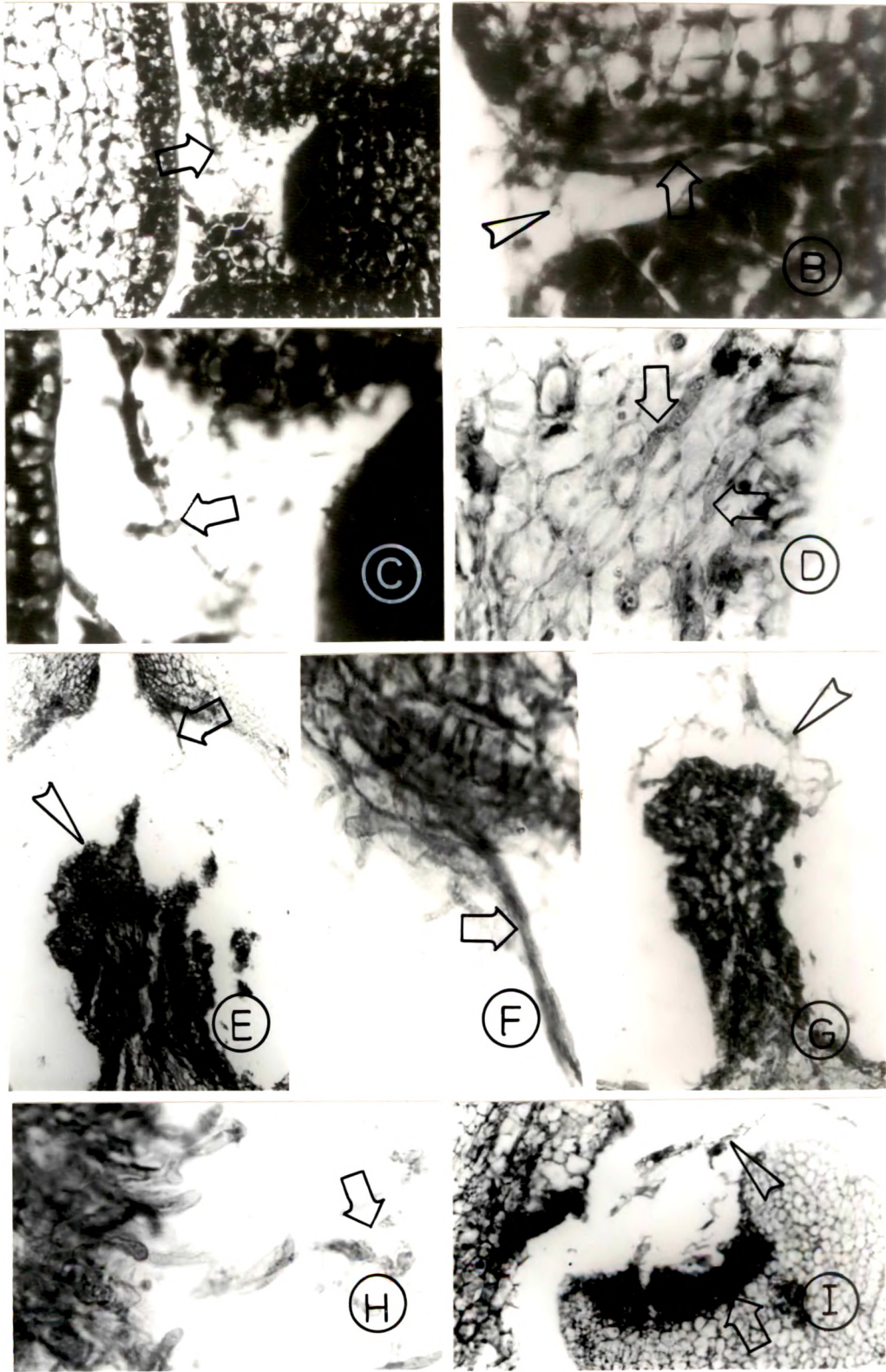


FIG.17

Fig.18. Transverse (A, B, E, G, H) and longitudinal sections (C, D, F,) of malformed panicle of cultivar Rajapuri.

- A Association of hyphal filaments (arrow) with the epidermal cell of peduncle. Note the dark phenolic contents (histochemical test for catechin derivates) (arrow head) in the cells close to the infection site. X158
- B Close view of cortical cells following histochemical staining for catechin contents (arrow) in the peduncle. X600
- C Anther filament showing distribution of starch granules (arrow). Note the fungal mat at the basal lobe of the anther (arrow head). X108
- D A locule of anther with pollen grains stained positive for starch deposits (arrow). X128
- E Epithelial cells (arrows) of pith ducts in peduncle showing positive reaction for proteins. X116
- F Cells in basal groove (arrow) of the anther lobe close to the filament attachment showing positive sites of portein accumulation. X430
- G Paratracheal parenchyma (arrow) showing lipid reserves in the peduncle. X545
- H Ray cells (arrow), phloem parenchyma showing positive sites of lipid accumulation in the peduncle. X138

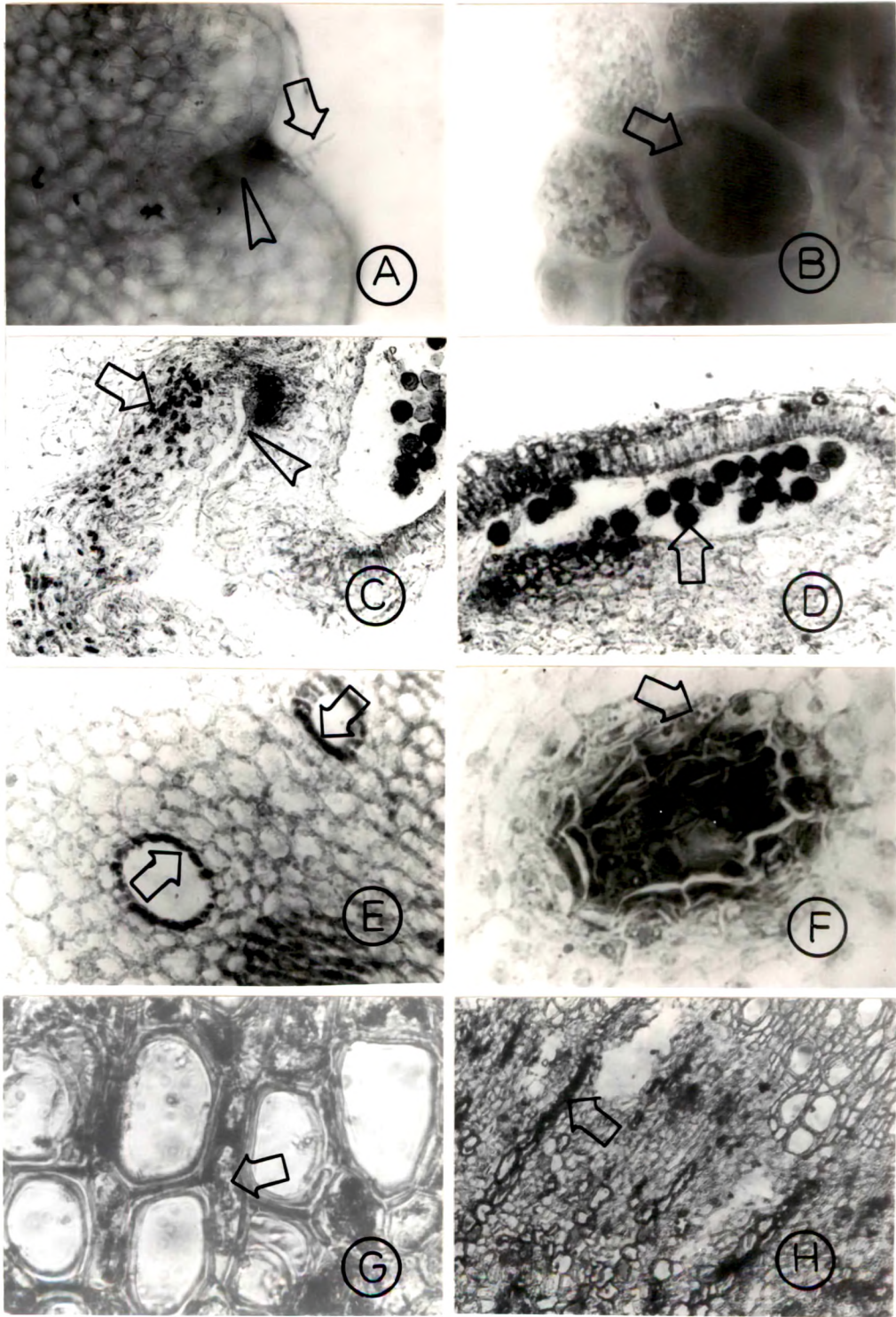


FIG. 18

Fig.19. Transverse (A-E and G,H) and longitudinal (F) sections of malformed floral tissues.

- A The gum-resin duct lumen filled with lipid secretion in the pedicel (arrow). X271
- B Cortical cells (arrow) of the peduncle showing granular precipitation of succinic dehydrogenase enzyme. X1100
- C Perivascular fibres in the cortex of peduncle showing succinic dehydrogenase activity in their lumen (arrow head). X900
- D Paratracheal parenchyma (arrow) showing dehydrogenase activity in the peduncle. X1000
- E Cortical cells of pedicel showing reaction product of SDH (arrow). X625
- F Anther epidermal (arrow) and inner cells of the basal lobe (arrow head) with no dehydrogenase activity. X775
- G The infection site of peduncle showing hypodermal cells (arrow) densely stained for the enzyme peroxidase. Arrow head indicates hyphal filaments. X151
- H A few parenchyma (arrow) next to the vessel elements with scanty reaction product of the enzyme peroxidase in the peduncle. X310

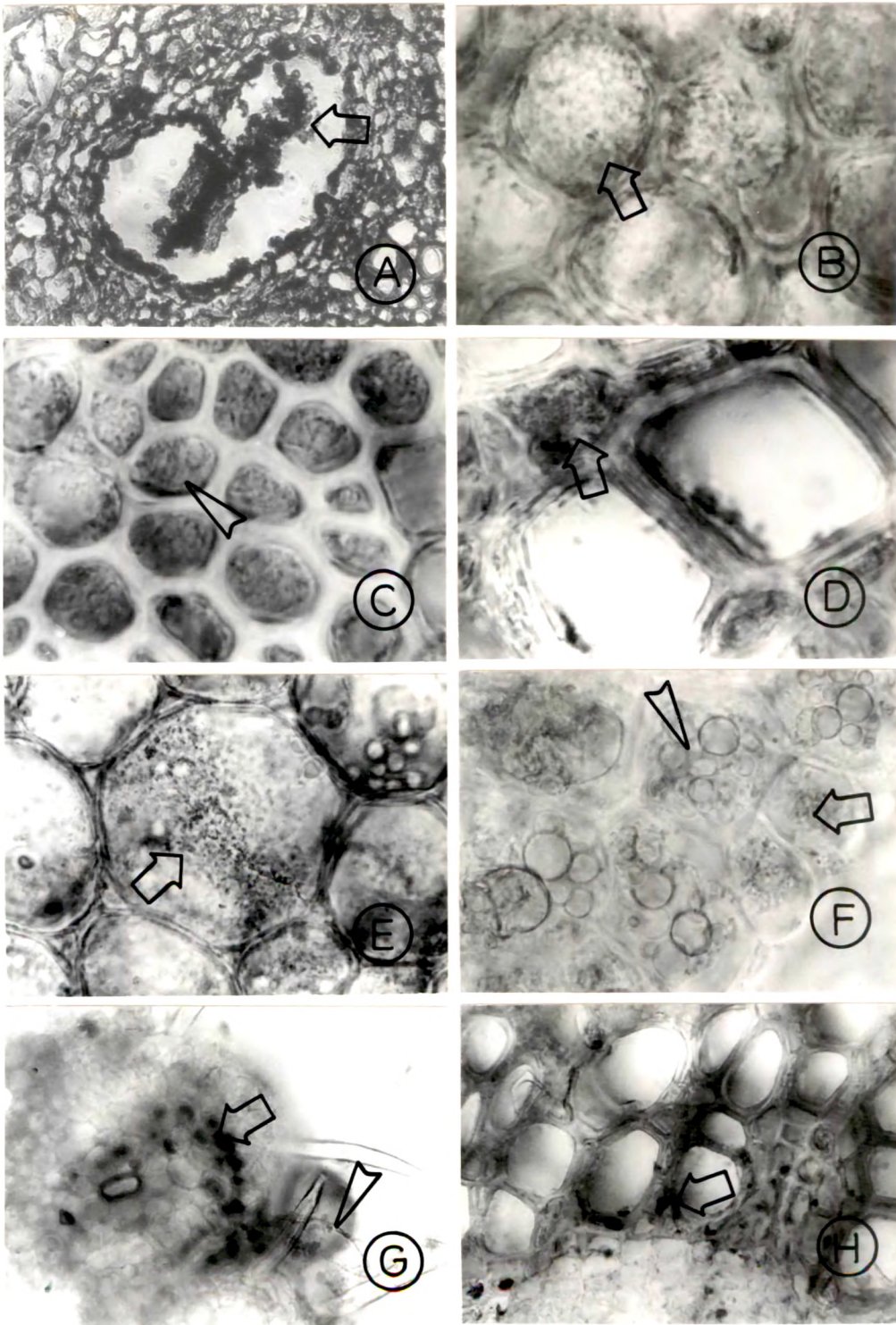


FIG.19

- Fig.20. Transverse (A,B,G, & H) and longitudinal (C-F) sections of malformed panicles of var. Rajapuri showing peroxidase enzyme localisation.
- A Pith parenchyma showing localised enzyme reaction product at the cell corners in the peduncle. X360
  - B The inner cortical cells (arrow) of the pedicel showing dense reaction of the enzyme at cell corners. X208
  - C An anther showing hyphal filaments (arrow) of the pathogen at the basal lobe and the reaction of the enzyme at the site (arrow head). X128
  - D Anther showing positive reaction of the enzyme along the cell walls. X320
  - E Style showing dense reaction product of the enzyme along the transmitting tissue (arrows). X108
  - F Ovule (ov) showing the intense peroxidase activity along the cell walls (arrow). X124
  - G Peduncle showing thin cuticle (arrow) on the epidermal cells. X700
  - H Gum-resin showing densely stained epithelial cells (arrows). X700

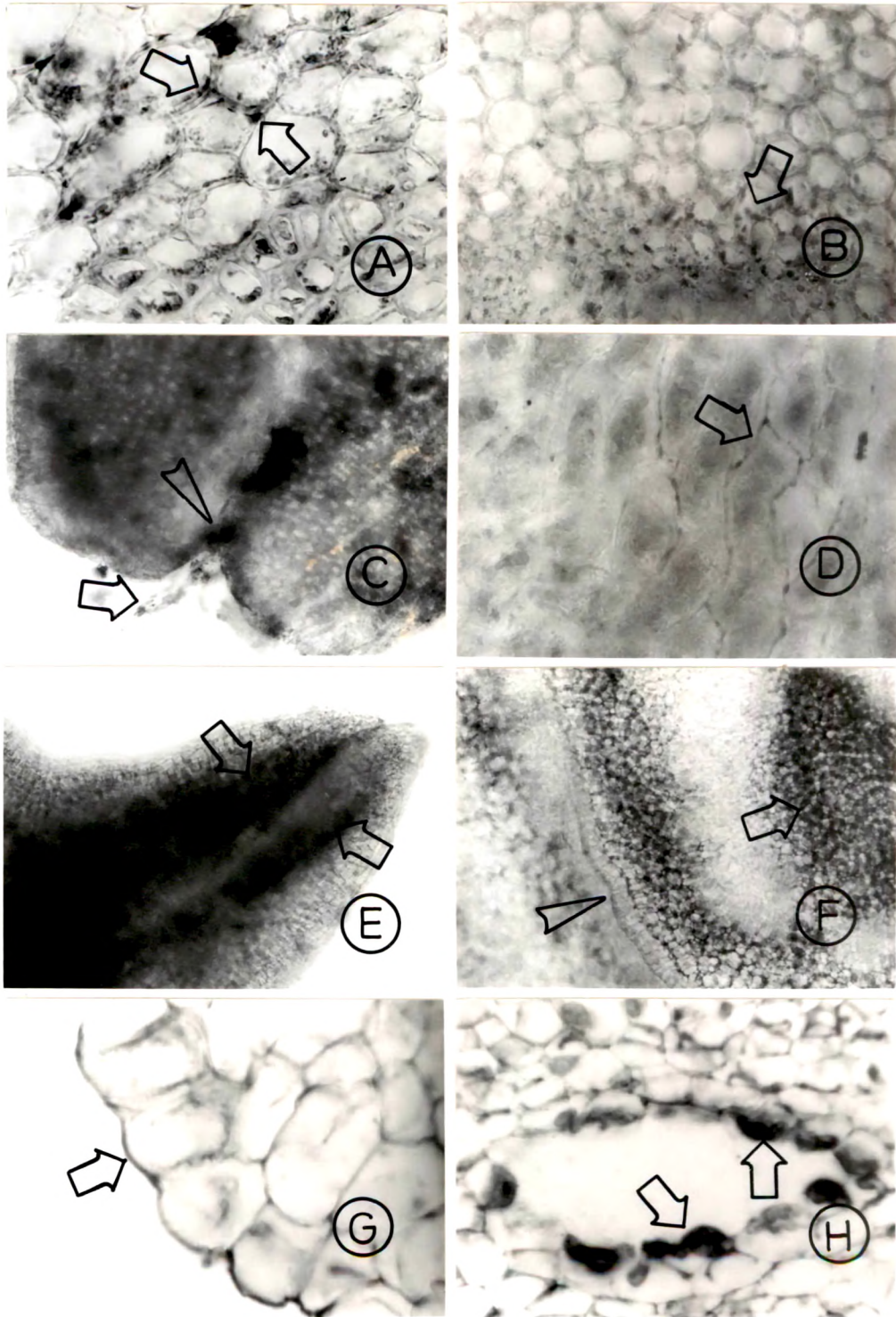


FIG.20

**Fig.21. Longitudinal (A and F) and transverse (B-E and G,H) sections of tissues from healthy panicles of variety Rajapuri.**

- A: Anther locule showing densely stained pollen grains and distinct tapetal cells (arrow). X1050**
- B Cortical cells showing distribution of starch granules (arrow) in the peduncle. X260**
- C Gum-resin duct of pith region of peduncle showing no proteinaceous secretion. X116**
- D Paratracheal parenchyma (arrow) of peduncle free of lipid bodies. X889**
- E Xylem ray cells (arrow) devoid of succinic dehydrogenase activity in the peduncle. X825**
- F The epidermal cells of the anther lobe showing dense (arrow) reaction sites of succinic dehydrogenase. X925**
- G Peduncle showing no peroxidase activity following heat treatment. X96**
- H Peduncle showing intense peroxidase activity (arrow) in the cortex (arrow head). X124**

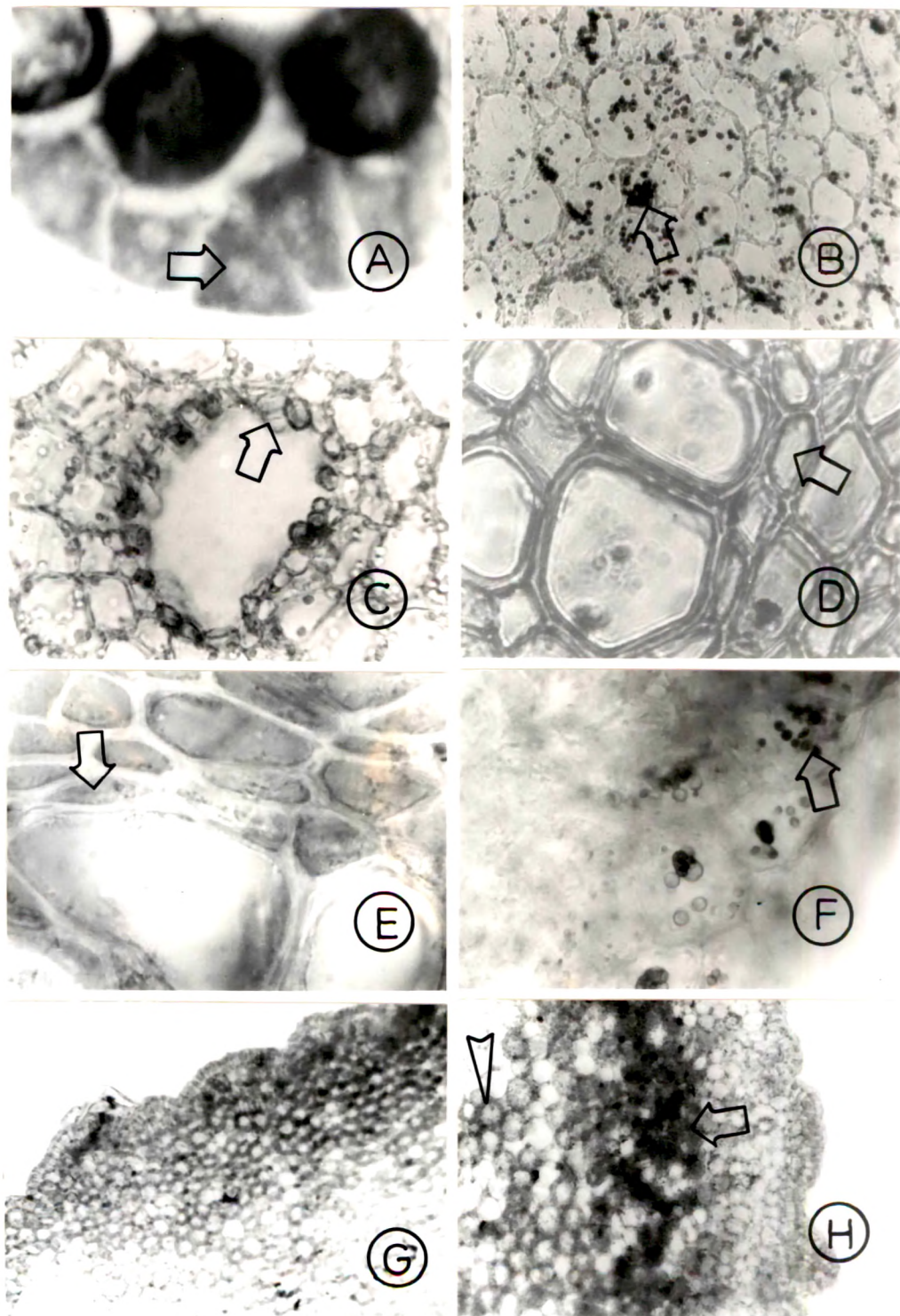


FIG.21

Fig.22. Transverse sections of healthy (A and B) and vegetatively malformed (C-I) tissues of var. Rajapuri.

- A Paratracheal parenchyma (arrow) devoid of peroxidase activity in the healthy peduncle. X470
- B Pith parenchyma of healthy peduncle showing peroxidase activity at cell corners (arrow). X220
- C Shoot showing distribution of sclerides in the cortex (arrow). X330
- D Unlignified perivascular fibres (arrow head) surrounding the gum-resin duct in shoot. X270
- E Xylem ray cells (arrow) showing dense granular stained material with toluidine blue. X300
- F Xylem ray cells (arrow) with no starch deposition. X300
- G Cortical cells showing distribution of proteins (arrow). X875
- H Gum-resin primary duct showing proteinaceous secretion (arrow). X600
- I Gum-resin secretion of primary duct showing lipid bodies (arrow). X625

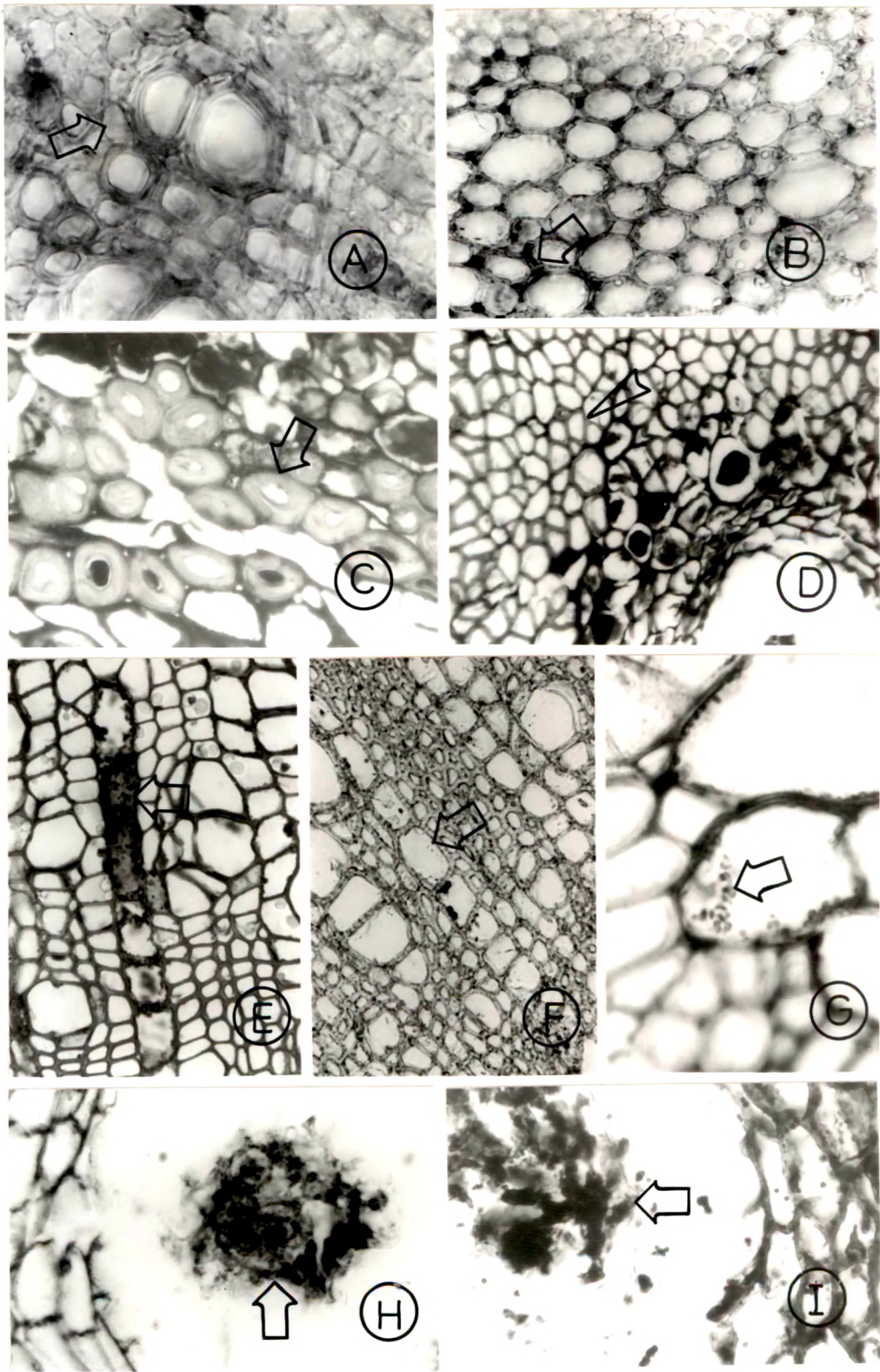


FIG. 22

Fig.23. Transverse (A-H) sections of vegetatively malformed shoots of var. Rajapuri.

- A Epidermal cells and outer cortical cells of shoot showing succinic dehydrogenase activity. X158
- B Paratracheal parenchyma showing distribution of lipids (arrow). X1050
- C Paratracheal parenchyma showing granular precipitation of succinic dehydrogenase enzyme (arrow) in shoots. X1025
- D Distribution of peroxidase activity in cortical parenchyma cells (arrow) in shoot. X250
- E Phloem parenchyma (arrow) showing dense reaction of peroxidase enzyme in the shoot. X100
- F Thick cuticle (arrow) covering the epidermis and extending into the radial walls of midrib of leaf. X750
- G Relatively thick walls (arrow) of vessel elements in the midrib of leaf. X725
- H Mesophyll of leaf lamina showing starch deposition restricted to spongy parenchyma (arrow). X1050

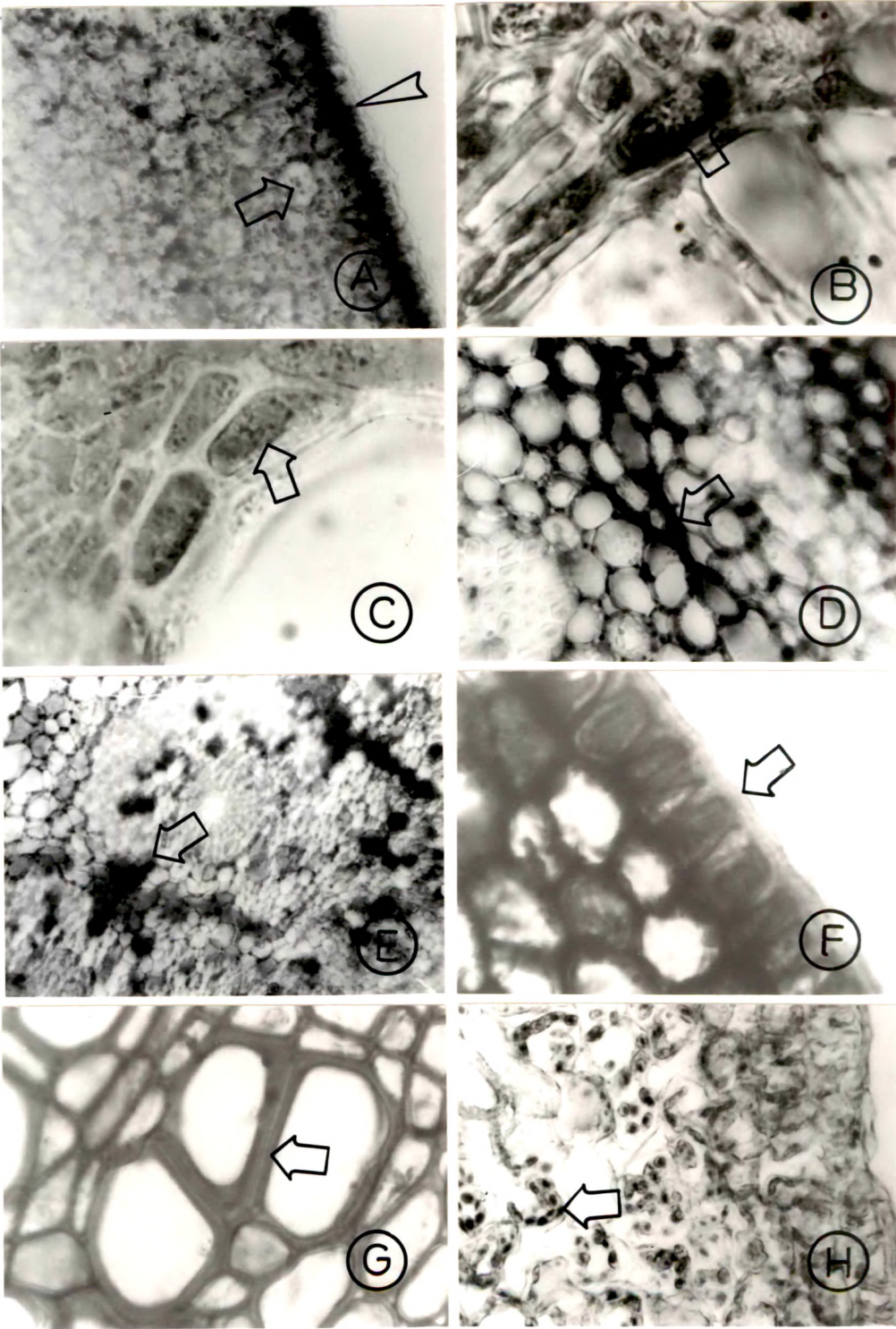


FIG.23

Fig.24. Transverse (A-H) sections of twigs of variety Rajapuri.

- A Palisade (arrow) and spongy parenchyma (arrow head) of leaf lamina showing protein deposition. X750
- B Ground parenchyma located around vascular tissue of leaf midrib showing lipid globules (arrow). X700
- C Dense stain representing succinic dehydrogenase enzyme activity in the palisade cells (arrow) in the midrib of vegetatively malformed leaf. X1025
- D Peroxidase enzyme activity along the vessel walls (arrow) and ground parenchyma (arrow head) in the midrib of vegetative malformed leaf. X158
- E Vegetative malformed leaf lamina showing intense reaction of peroxidase activity on lower (arrow) and upper epidermis (arrow head). X158
- F Healthy shoots showing thick walled lignified sclerids in the cortex (arrow). X330
- G Lignified perivascular fibres (arrow head) surrounding the gum-resin duct in healthy shoot. X270
- H Xylem ray cells of healthy shoot showing abundant starch grains (arrows). X300

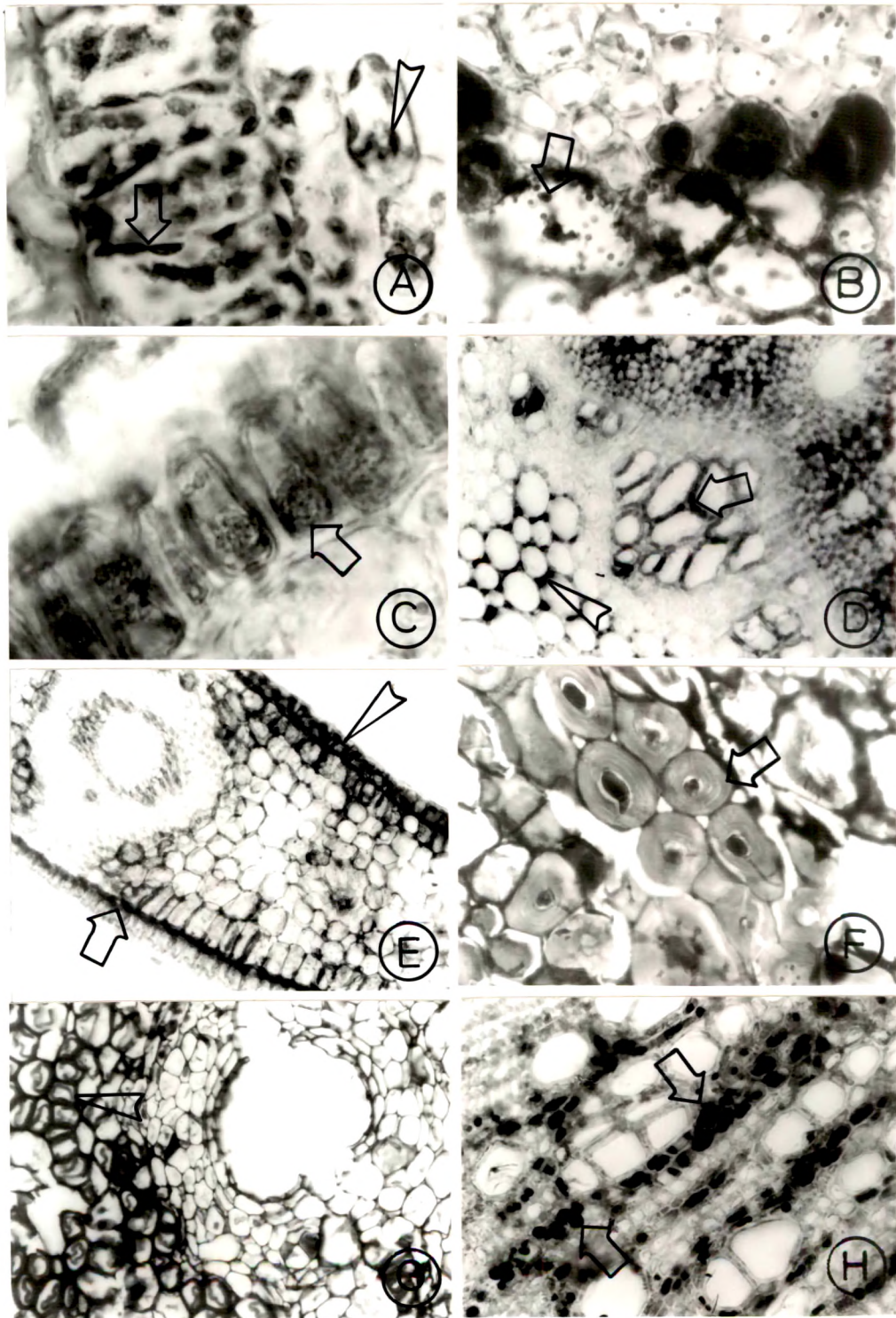


FIG. 24

- Fig.25. Transverse (A-H) sections of healthy twigs of variety Rajapuri.
- A Cortical cells of shoot showing protein deposits (arrow). X775
  - B Paratracheal parenchyma of healthy shoots showing no deposition of lipid bodies (arrow). X875
  - C Paratracheal parenchyma (arrow) showing no reaction for succinic dehydrogenase enzyme in shoot. X875
  - D The cortical parenchyma (arrow) of shoot showing scanty peroxidase activity. X100
  - E Relatively thin cuticle (arrow) covering the epidermis in the mid rib of leaf. X700
  - F Starch deposition restricted to spongy parenchyma (arrow) in the mesophyll of leaf. X750
  - G Vessels (arrow) and ground parenchyma (arrow head) showing less activity of peroxidase enzyme in the mid rib of leaf. X151
  - H Peroxidase enzyme activity restricted only to the lower epidermal cells (arrow) of healthy leaf. X158

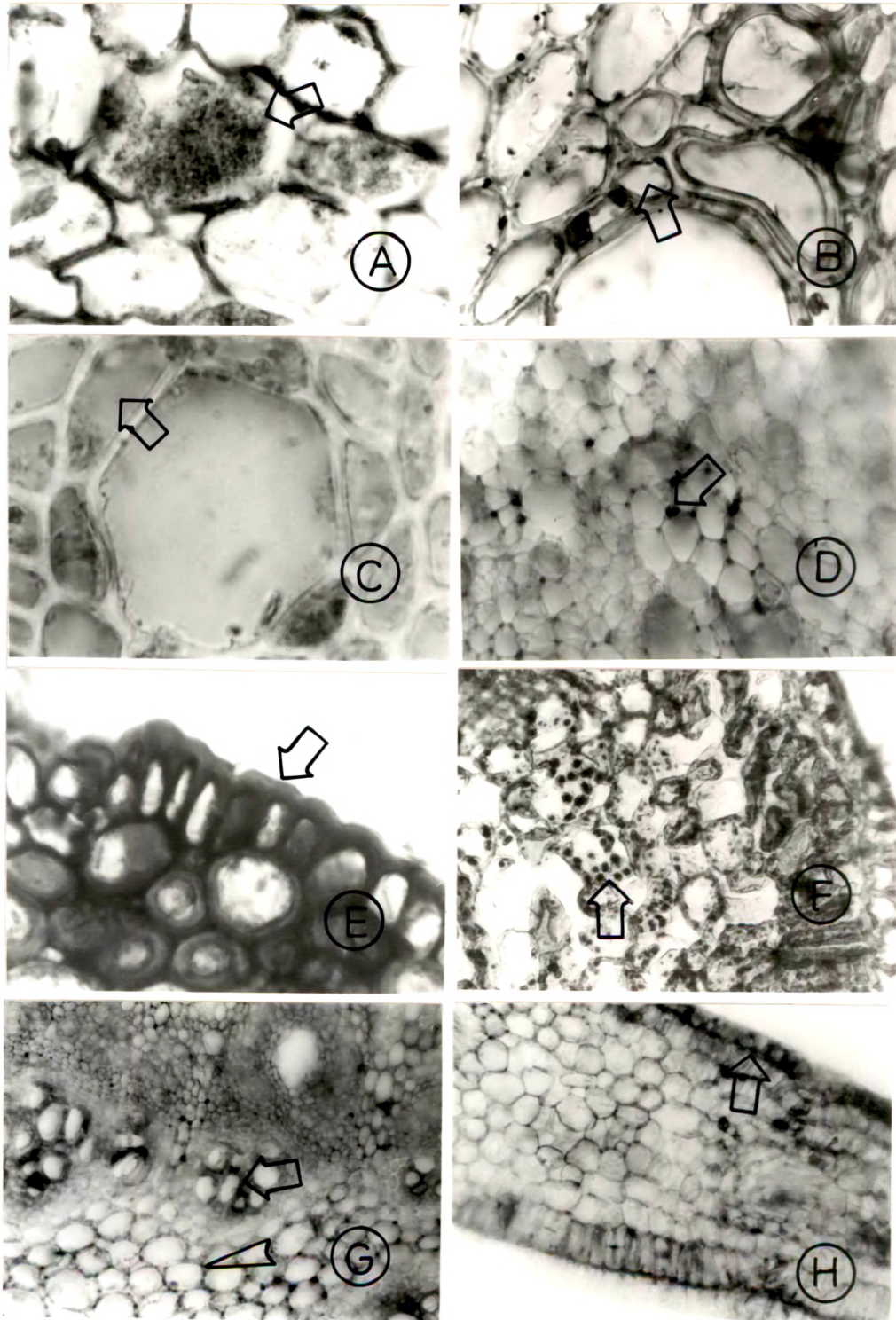


FIG.25

Fig.26. Transmission electron micrographs of ultrathin sections of young and mature anthers from malformed panicles.

- A Hyphal fragments (arrow) of *Fusarium moniliforme* seen close to anther in a young bud. x3770
- B Tapetal cells (arrow) showing vacuolated electron dense cytoplasm adjacent to microspore mother cells (M). X2106
- C Microspore mother cell of young anther showing electron dense substances and lipid globules (L). X7540
- D Vesciculated endoplasmic reticulum (arrow) of the tapetal cells surrounding large vacuoles in young anther. X21320
- E Tapetal cells of young anther showing electron dense cytoplasm with a vacuole containing vescicular bodies (arrow). X14700
- F A large vacuole in the tapetal cells of young anther showing a electron dense globular body and membranous structures (arrow). X29400
- G The cytoplasm of microspore mother cell showing globular and spindle shaped electron dense structures and lipid globules (L). X7540
- H Basal portion of mature anther showing fragments of hyphae (arrow) close to the epidermal cells. X3625

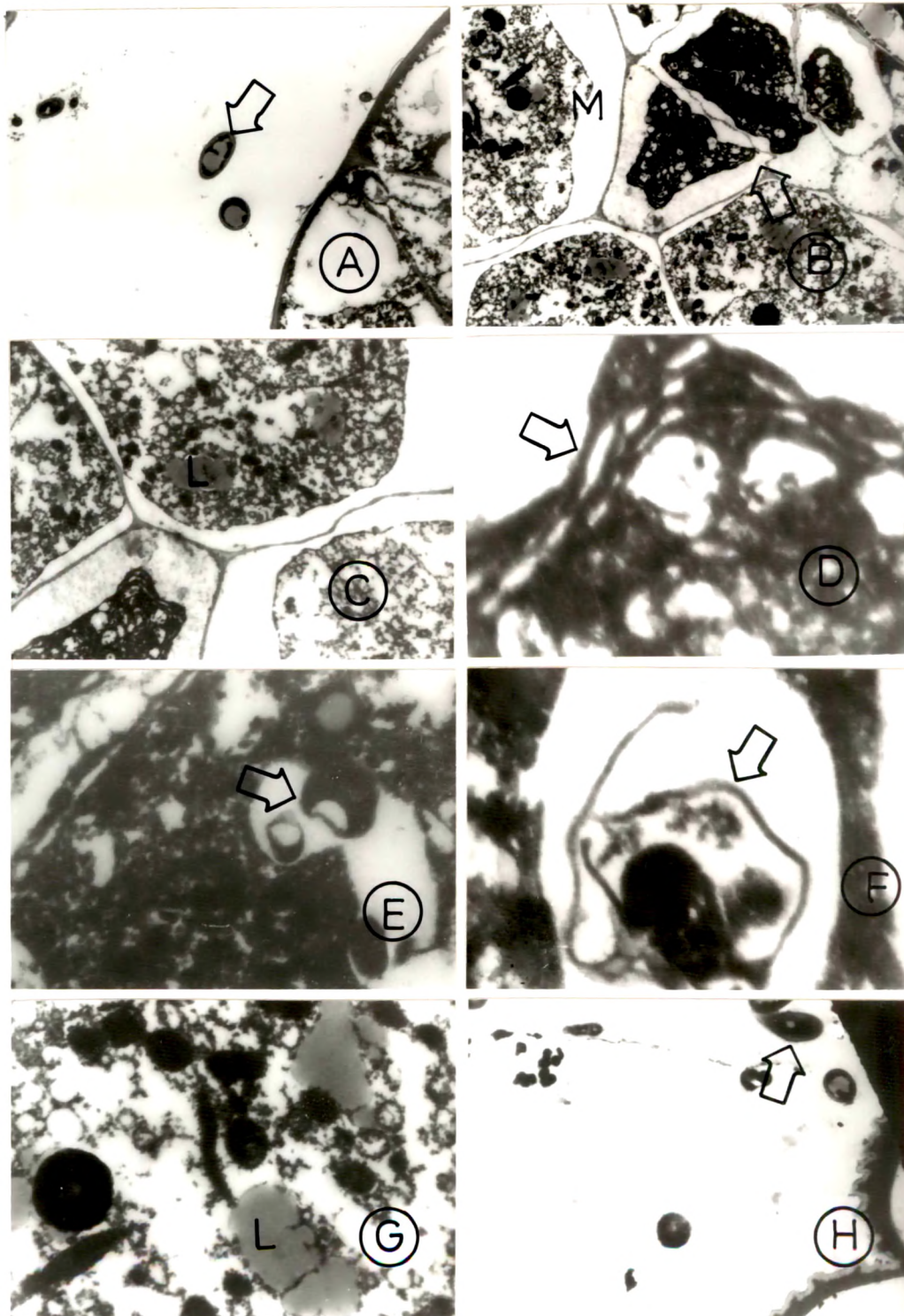


FIG.26

Fig.27. Transmission electron micrographs of mature anthers from malformed flowers.

- A Serrated thick cuticle (arrow) covering the basal epidermal cells with electron dense cytoplasm (arrow head). X7830
- B Intracellular hyphae (arrow head) alongwith electron-dense material in the inner cells of the basal epidermis. X5535
- C Some of the anther cells close to the connective showing intracellular hyphae (arrows). X2875
- D A close view of the intracellular hyphal filament (arrow) near connective. X15120
- E A tracheary element in the connective showing secondary wall thickening (arrows) and electron dense material in the cell lumen. X8120
- F A parenchyme cell next to a trachery element with electron dense material (arrow head). X8120

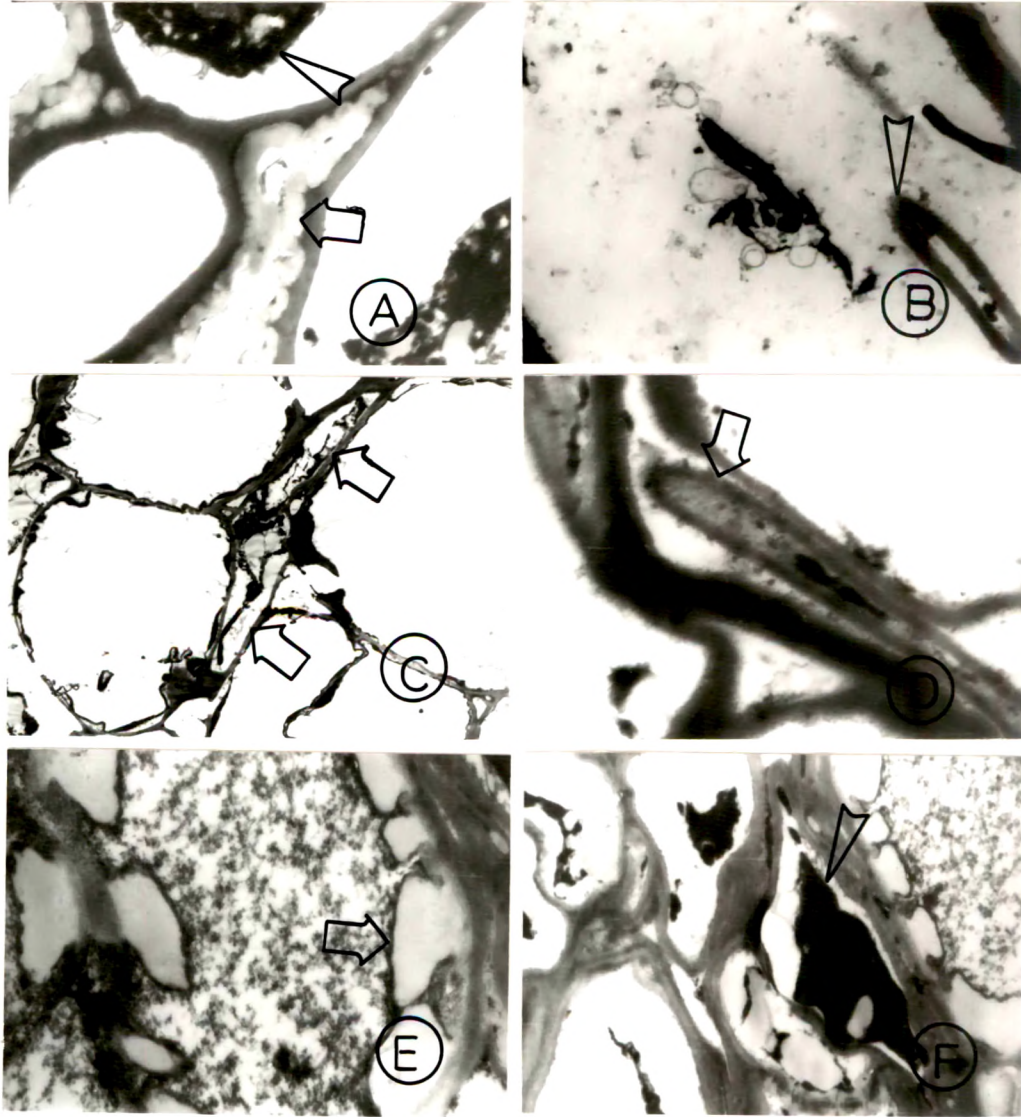


FIG. 27

Fig.28. Transmission electron micrographs of stylar region, ovary wall and ovule of flowers from malformed panicles.

- A Stylar transmitting tissue cell showing large lipid body (L) surrounded by numerous vacuoles (V) and dark contents. X11760
- B Cells of transmitting tissues showing thick irregular cell walls and electron dense cytoplasm. X11760
- C Cells of transmitting cells showing thick irregular cell walls with intercellular space (arrow). X21000
- D The inner layers of ovary wall showing disrupted cells with thickened walls (arrow) and electron dense cytoplasm (arrow head). X2106
- E Cells from outer surface of the ovule near chalazal end showing attachment of conidia like structure (arrow head). Note the cells containing electron dense material and irregular vacuoles (arrow). X2187
- F Magnified view of Fig. E. showing Conidia-like structure (arrow). X4785
- G Ovule surface with macroconidia-like structures of *F. moniliforme* (arrow) lying close to the host cells. Note the host cell filled with extensive electron dense material and large vacuoles. X4785
- H Intracellular hyphal fragment (arrow) in the inner ovule cells with electron dense substance along the inner side of cell wall. X7965

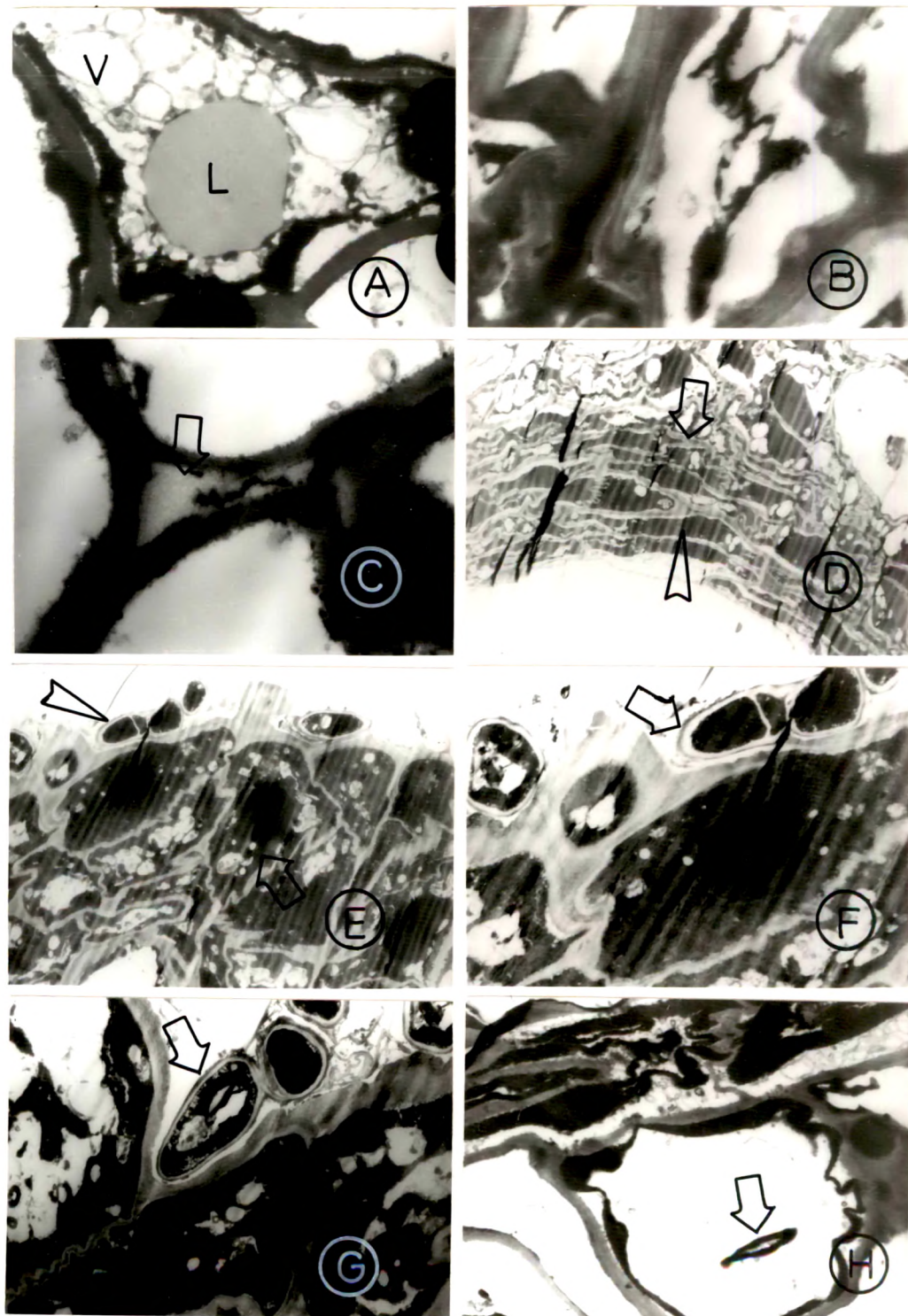


FIG.28

Fig.29. Scanning electron micrographs of sepals and anthers

- A A portion of sepals from malformed flowers showing thick mycelial mat (arrow) attached on its ventral surface. X3120
- B Surface of healthy anther showing grooved epidermal cell walls (arrow head). X2600
- C Anther of a flower from a malformed panicle with no distinct grooves. Note the association of mycelial mat with anther wall (arrow). X2600
- D Anther of diseased flower showing association of hyphal filaments with the basal cells where the filament is attached (arrow). X650
- E&F Enlarged view of Fig. D showing mycelial mat attached to the basal cells of the anther. (Fig. E. X 2600 & Fig. F. X5200)
- G Terminal portion of the anther showing fungal filament (arrow) between two anther lobes of diseased flower. X910
- H Irregularly shaped pollen grains from anthers of flowers from malformed panicle. X2600

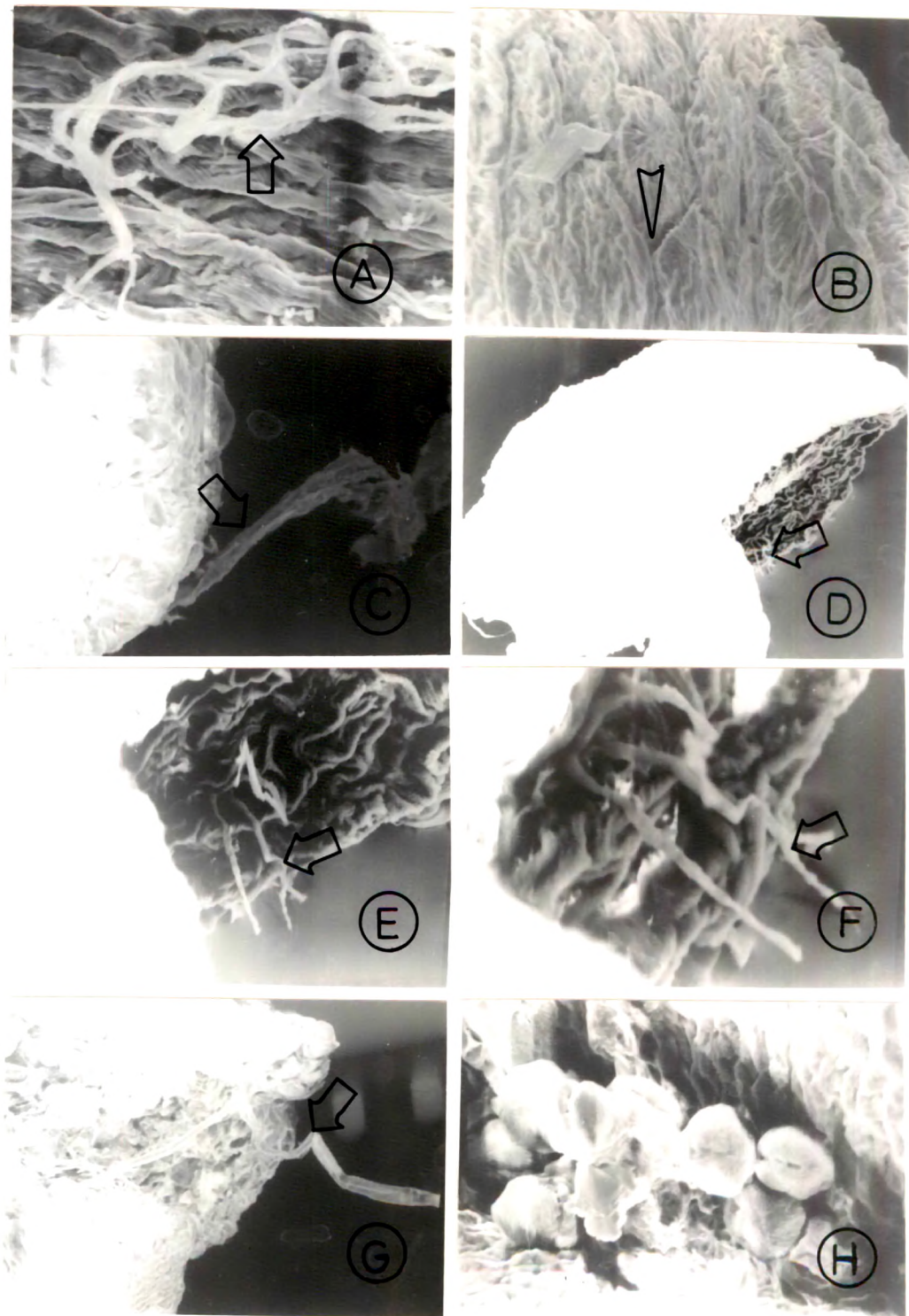


FIG. 29